Low-Temperature Plasticity and Dislocation Creep of Fangshan Dolomite

Article *in* Journal of Geophysical Research: Solid Earth · May 2021

DOI: 10.1029/2020JB021439

4 authors, including:

Jianfeng Li
Chinese Academy of Sciences
17 PUBLICATIONS **43** CITATIONS
SEE PROFILE

Tongbin Shao
China Earthquake Administration
35 PUBLICATIONS **464** CITATIONS
SEE PROFILE

Maoshuang Song
Chinese Academy of Sciences
62 PUBLICATIONS **1,198** CITATIONS
SEE PROFILE

JGR Solid Earth

RESEARCH ARTICLE
10.1029/2020JB021439

Low-Temperature Plasticity and Dislocation Creep of Fangshan Dolomite

Jianfeng Li[1,2], **Tongbin Shao**[1,2], **Maoshuang Song**[1,2], **and Hao Wang**[1]

[1]State Key Laboratory of Isotope Geochemistry, Guangzhou Institute of Geochemistry, Chinese Academy of Sciences, Guangzhou, China, [2]CAS Center for Excellence in Deep Earth Science, Guangzhou, China

Key Points:

- Low-temperature plasticity and dislocation creep of dolomite were recognized at $T \leq 500$°C and $T \geq 800$°C, respectively
- Stress exponent ($n = 4.75$) and activation energy ($Q = 436$ kJ/mol) were determined for the dislocation creep of Fangshan dolomite
- Q for dislocation creep is not only higher than that for diffusion creep, but also is comparable to the values of calcite and magnesite

Correspondence to:
T. Shao and M. Song,
tshao@gig.ac.cn;
msong@gig.ac.cn

Citation:
Li, J., Shao, T., Song, M., & Wang, H. (2021). Low-temperature plasticity and dislocation creep of Fangshan dolomite. *Journal of Geophysical Research: Solid Earth*, *126*, e2020JB021439. https://doi.org/10.1029/2020JB021439

Received 28 NOV 2020
Accepted 7 APR 2021

Abstract To explore the rheology of dolomite and investigate recent findings regarding the so-called inversion of activation energy between dislocation and diffusion creep, we compressed medium-grained Fangshan dolomite (113 ± 42 μm) at effective confining pressures of 50–300 MPa, temperatures of 27°C–900°C, and strain rates of 10^{-6} to 2×10^{-4} s^{-1} using a Paterson gas-medium apparatus. Two end-member deformation regimes with corresponding diagnostic flow laws and microstructures were identified. At temperatures ≤500°C, low-temperature plasticity (LTP), which is characterized by microstructures of predominant abrupt undulatory extinctions and f-twins, was determined to dominate the deformation of Fangshan dolomite. The corresponding flow behavior can be described by an $\dot{\varepsilon} = \dot{\varepsilon}_0 \times \exp(\alpha \times \sigma)$ with $\alpha = 0.0806 \pm 0.0078$ and $\ln \dot{\varepsilon}_0 = -76.66 \pm 6.24$ (Regime 1). At temperatures ≥800°C, dislocation creep, which shows characteristic microstructures of smooth undulating extinction and new recrystallized grains, dominated the deformation of Fangshan dolomite. The corresponding flow behavior can be expressed by a power law equation, $\dot{\varepsilon} = A\sigma^n \exp\left(\frac{-Q}{RT}\right)$ with $n = 4.75 \pm 0.58$, $Q = 436 \pm 54$ kJ/mol, and $\log A = 3.48 \pm 1.41$(Regime 2). At temperatures between ~500 and 800°C, a transition regime between LTP and dislocation creep was identified (Regime 3) with the dependence of flow stress on strain rate increasing gradually with increasing temperature. When extrapolated to natural conditions, our flow law of dislocation creep for dolomite in combination with that of diffusion creep reported by Davis et al. (2008) suggests that the dislocation creep regime of dolomite is limited to a relatively narrow region of high temperature and relatively high stress, whereas the diffusion creep regime dominates the deformation of dolomite in tectonic settings with low stress levels.

1. Introduction

Carbonates, which commonly form and accumulate in shallow marine environments along continental margins, comprise 10%–35% of sedimentary rocks on the Earth's surface. They are distributed extensively in orogenic belts and are involved in structural deformation in the middle and upper crust during the process of continental collision and orogenesis. Carbonates are also important components of ultrahigh-pressure (UHP) metamorphic terranes. Some carbonates may even exist at the depths of the upper mantle and the mantle transition zone (Brenker et al., 2007; Goto et al., 2007; Thomson et al., 2016; Zhang et al., 2003). Due to their low flow stress, carbonate phases such as calcite ($CaCO_3$) and dolomite [$CaMg(CO_3)_2$] are believed to sustain large strains and control the stresses generated by deformation in the middle and upper crust during continental collision (e.g., Bestmann et al., 2000; Ulrich et al., 2002) and play a crucial role in the geodynamic processes of UHP metamorphic terranes, mantle wedges, and subducted slabs (Holyoke et al., 2014a). Therefore, it is of great importance to study the mechanical properties of all carbonates, especially the $MgCO_3$-$CaCO_3$ system, to understand the strain and stress distributions and geodynamic processes in orogenic belts and subduction zones.

Many experimental and geological observations have revealed that carbonates, which normally form at shallow depths on Earth, can be transported to the deep mantle in subduction zones. Several carbonate phases are commonly found in natural carbonate rocks, including Ca end-member carbonate, calcite, Mg end-member carbonate, magnesite, and dolomite, which has intermediate (Mg:Ca = 1:1) mineral compositions. Carbonate rocks composed of primarily calcite and/or dolomite are important constituents of exhumed UHP metamorphic terranes in orogenic belts and often contain high-pressure metamorphic rocks (e.g., eclogite) and minerals (e.g., garnet, coesite, and diamond), which record the *P-T* history that these

carbonate rocks experienced during subduction and exhumation processes. In particular, the decomposition reaction of dolomite → magnesite + aragonite observed in western Tianshan, China, and in the Kokchetav massif of northern Kazakhstan indicates that dolomitic marbles reached depths of 150–280 km during subduction (Buob et al., 2006; Luth, 2001; Sato & Katsura, 2001; Shirasaka et al., 2002; Zhang et al., 2003; Zhu et al., 2002). The brucite/calcite intergrowths [$Mg(OH)_2/CaCO_3$] observed in mantle-derived xenoliths from the kimberlite pipes of Kimberley, South Africa, indicate the existence of relatively abundant dolomite in the source region of the upper mantle (Berg, 1986). Calcite and walstromite-structured $CaSiO_3$ inclusions, which are found in ultradeep diamonds from Juina, Brazil, indicate that carbonates in subducting slabs may reach the lower part of the mantle transition zone (Brenker et al., 2007). Calcite and dolomite can react with peridotite to transform into dolomite and magnesite at 1–4 GPa (Eggler et al., 1976; Wyllie & Huang, 1976), and it is predicted that carbonates may exist in the forms of dolomite and magnesite in the deep mantle. Experimental studies on the phase stability of dolomite and magnesite suggest that these two carbonate phases, although undergoing some structural modifications under compression, can remain chemically stable under normal mantle geotherms, with dolomite reaching the middle-lower mantle and magnesite reaching the core-mantle boundary (Isshiki et al., 2004; Merlini et al., 2012).

In recent decades, the rheological behavior and deformation mechanisms of calcite, including single crystals and polycrystalline aggregates, have been investigated extensively (e.g., Austin & Evans, 2009; de Bresser, 2002; de Bresser et al., 2005; Freund et al., 2004; Gratier et al., 2011; Griggs et al., 1953; Griggs & Miller, 1951; Handin & Griggs, 1951; Heard & Raleigh, 1972; Herwegh et al., 2005, 2003; Renner et al., 2002; Rutter, 1972, 1974; Rybacki et al., 2013, 2011; Schmid et al., 1980, 1977; Song et al., 2014; Turner et al., 1956; Walker et al., 1990; Xu et al., 2010, 2009; Zhang et al., 2017; Zhang & Zhou, 2012). In contrast to calcite, few high-temperature deformation experiments have been performed on dolomite and magnesite, limited to a few experimental studies on the deformation of dolomite reported for both single crystals (e.g., Barber et al., 1981; Barber & Wenk, 1979, 2001) and polycrystalline aggregates (e.g., Davis et al., 2008; Delle Piane et al., 2008; Heard, 1976; Holyoke et al., 2013; Neumann, 1969). Early experimental deformation studies on dolomite mainly focused on the deformation mechanisms and microstructural analysis under a restricted set of experimental conditions; however, flow laws were not well established due to the low stress resolution of the solid-medium Griggs deformation apparatus. In addition, these studies provided little evidence of dislocation and diffusion creep for dolomite. In recent years, the rheological behavior of dolomite aggregates has been systematically investigated over a wide range of confining pressures, strain rates, and temperatures using deformation apparatuses with high stress resolutions, including Heard-type gas-medium apparatuses, Paterson gas-medium apparatuses, and Griggs-type deformation apparatuses using improved low friction cells (Davis et al., 2008; Delle Piane et al., 2008; Holyoke et al., 2013, 2014a, 2014b). Three types of deformation mechanisms—low-temperature plasticity (LTP), dislocation creep, and diffusion creep—have been identified, and the flow laws associated with these mechanisms have been determined.

Owing to the complex deformation behavior of dolomite, some open questions remain. Previous experimental studies of dolomite LTP have revealed a highly nonlinear relationship between stress and strain rate and an anomalous increase in plastic flow strength with increasing temperature (Barber et al., 1981; Davis et al., 2008; Higgs & Handin, 1959). Experimental studies of dislocation creep of coarse-grained dolomite report different flow parameters due to the limited range of conditions over which dislocation creep is predominant. Davis et al. (2008) first quantified the dislocation creep of dolomite by conducting triaxial compression experiments on coarse-grained Madoc dolomite (240 ± 30 μm) in a Heard-type gas-medium apparatus at temperatures of 400°C–850°C and effective confining pressures of 50–400 MPa. The value of activation energy they reported was $Q = 410$ kJ/mol for dislocation creep. Due to the limited mechanical data that they collected, they derived the activation energy for dislocation creep with an assumed stress exponent $n = 7$. However, as pointed out by Holyoke et al. (2013), Davis et al. (2008) were unable to explore the dislocation creep of dolomite in detail, and their mechanical data were transitional between LTP and dislocation creep. Holyoke et al. (2013) further investigated the dislocation creep of dolomite by conducting triaxial compression experiments at temperatures of 700°C–1,000°C and effective pressures of 300–900 MPa in a Griggs-type deformation apparatus. The activation energy value of dolomite dislocation creep was determined to be 145 kJ/mol with a stress exponent $n = 3$, which is much lower than that reported by Davis et al. (2008) and even lower than the activation energy value of dolomite diffusion creep (Davis et al., 2008; Delle Piane et al., 2008). Because the rate-limiting mechanisms of intracrystalline deformation

Table 1
Chemical Composition (wt %) of Fangshan Dolomite

Point#	MgO	CaO	FeO	Al_2O_3	Na_2O	MnO	P_2O_5	TiO_2	Total	Mg/Ca
1	20.61	29.88	0.12	0.00	0.02	0.00	0.01	0.00	50.65	0.97
2	21.18	30.25	0.11	0.02	0.04	0.00	0.01	0.03	51.64	0.98
3	21.41	29.38	0.11	0.02	0.07	0.03	0.00	0.00	51.02	1.02

are controlled by a larger energy landscape (activation barriers) relative to grain boundary processes such as grain boundary sliding and diffusion creep (Poirier, 1985), it is generally accepted that the activation energy of dislocation creep is normally higher than that of diffusion creep for most minerals. Therefore, the inversion of activation energy between dislocation and diffusion creep for dolomite is quite unusual, and it is necessary to further explore the dislocation creep of dolomite to understand the cause behind the inversion of activation energy between dislocation and diffusion creep.

This paper reports new experimental results for the LTP and dislocation creep of Fangshan dolomite with a grain size (113 ± 12 μm), which is intermediate to those of natural and synthetic dolomites (240 ± 30 and 2.5 ± 1.5 μm, respectively) deformed experimentally in prior studies (e.g., Davis et al., 2008; Holyoke et al., 2013). We noticed that the differing reported flow law parameters for dislocation creep of dolomite might arise mainly from problems in characterizing the small field of dislocation creep. By choosing medium-grained Fangshan dolomite as the starting material, the transition temperature between the LTP and dislocation creep fields of deformation could be shifted significantly to lower temperatures than coarse-grained Madoc dolomite. Hence, dislocation creep of dolomite could be observed and measured over an expanded wider range of temperature conditions, allowing us to more reasonably determine the flow law of dislocation creep for dolomite aggregates.

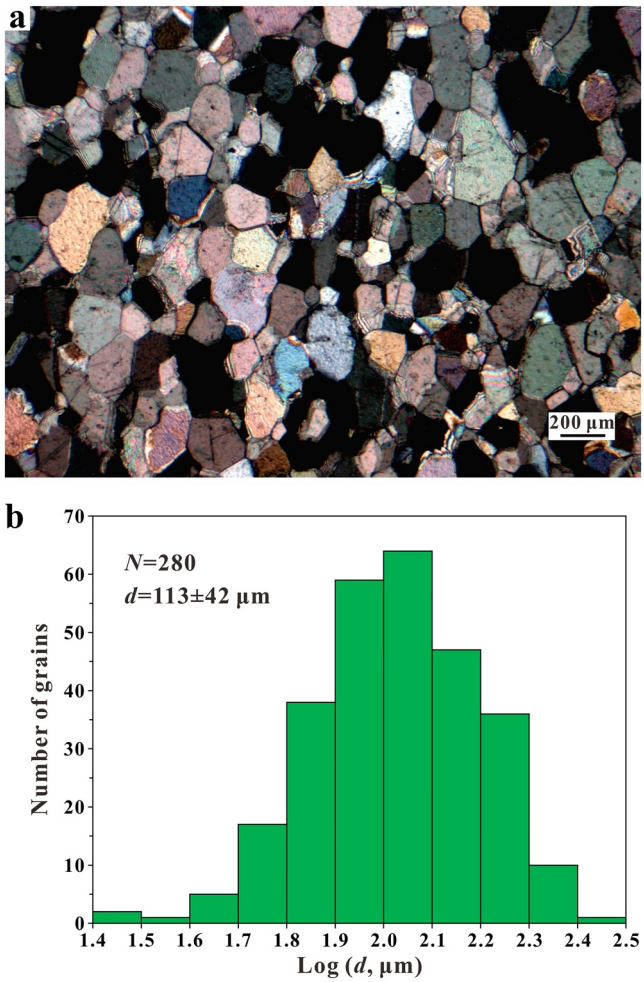

Figure 1. (a) Optical micrograph of cross-polarized light and (b) frequency histogram of grain size for the undeformed Fangshan dolomite starting material. The starting material is composed of approximately equant grains of dolomite with an average diameter of ~113 ± 42 μm and is characterized by sharp grain boundaries, uniform extinction, and some twins.

2. Experimental Methods

A series of triaxial compression experiments were conducted on natural Fangshan dolomite aggregates to determine the dependencies of flow stress on strain rate and temperature. The microstructures of the starting material and deformed samples were examined by optical observation of ultrathin polished sections (~10 μm) under a Leica optical microscope. Scanning electron microscopy (SEM) was used to characterize the fine-grained materials produced at high temperatures. The chemical composition of minerals was determined by electron microprobe analysis (EMPA).

2.1. Starting Material

A white block of dolomite was collected from a quarry located in Shiwo town, Fangshan district, Beijing, China. The block was homogenous in structure with no obvious mineral bands or foliations and contained primary dolomite (>97 vol %), secondary calcite, mica, and apatite. According to the EMPA results, the chemical composition of the dolomite minerals had a stoichiometric molecular formula with Mg/Ca ratios between 0.97 and 1.02 (Table 1). Optical examination indicated that this starting material had approximately equant grains (Figure 1a) with a grain size of 113 ± 42 μm in diameter; here, the grain size was the mean chord length determined by linear traverses of the optical microscopy images of

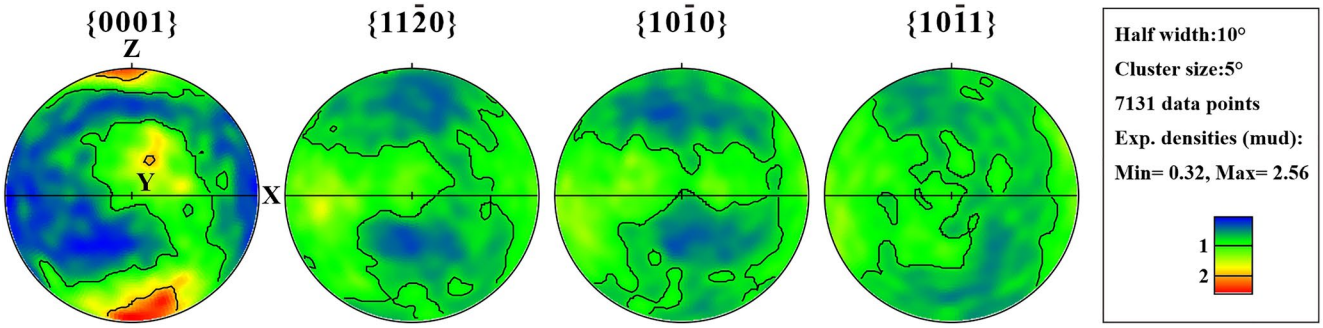

Figure 2. Pole figures of the starting material indicating a weak fabric of the *c* and *a* axes dolomite crystals.

thin sections (Figure 1b). Under crossed-polarized light, sharp grain boundaries, uniform extinction, and some straight boundary twins can be observed (Figure 1a). Based on optical observations and a comparison between the density of dolomite and the density calculated for cylinder samples using the determined mineral composition, the material was estimated to have a negligible porosity (less than 1%). Although neither banding nor foliation was visually detected in the specimens, the pole figures (Figure 2) generated by electron backscatter diffraction (EBSD) analysis revealed a weak initial fabric with maximum *c* axis densities of dolomite approximately two times the expected mean density for uniform distributions.

2.2. Sample Preparation and Jacketing

The specimens used for the deformation experiments were prepared in a cylindrical shape with a 10 mm diameter and a 20 mm length by core-drilling the block of Fangshan dolomite and machining by a lathe. The two end surfaces of the dolomite cylinders were optically polished to a roughness of less than ±5 μm. Before each deformation experiment, the cylindrical specimens were dried at 110°C for at least 24 h in an oven to remove free water. Then, a dried sample was sandwiched between two 3 mm thick solid alumina spacers, an additional two 58 mm long alumina pistons and two 30 mm long zirconia pistons (Figure 3). The assembly was inserted into a low-carbon iron jacket with a 0.25 mm wall thickness and a 15 mm inner diameter to isolate the sample from the confining pressure medium, which was argon gas. To fit the size of the cylindrical specimens, the central part of the iron jackets was cold swaged down to 10 mm in diameter, resulting in local thickening up to a maximum wall thickness of ~0.4 mm.

2.3. Deformation Experiments

Triaxial compression experiments were performed on dolomite aggregates under effective confining pressures of ~50–300 MPa, temperatures of ~27°C–900°C and strain rates of 1×10^{-6} to 2×10^{-4} s^{-1} in an internally heated Paterson gas-medium (argon) deformation apparatus (Paterson, 1970; Shao et al., 2011). The temperature distribution inside the furnace was routinely calibrated to ensure that the temperature

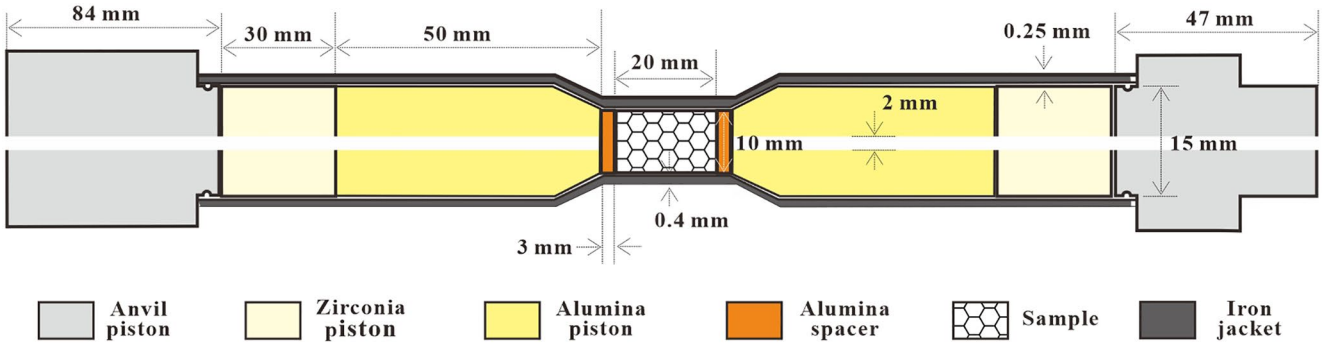

Figure 3. Schematic diagram of the sample assembly for triaxial compression experiments in a Paterson-type deformation apparatus.

over the central area (hot zone) of the thermal profiles was nearly constant with a gradient less than ±2°C along the length of the sample. The temperatures were controlled and monitored by an R-type (Pt13%Rh-Pt) thermocouple placed in contact with the upper surface of the upper alumina spacer, which was approximately 3 mm above the top surface of the sample. During the deformation experiments, the temperature was first increased at a rate of ~20°C per minute to the testing temperature and maintained for 30 min until equilibrium was reached; then, the sample was deformed. Deformation experiments were carried out by controlling the strain rate in two ways: constant-strain rate and strain-rate stepping. The strain-rate-stepping experiments were mainly aimed at detecting the dependence of flow stress on strain rate because such experiments can eliminate the effect of the microstructure by using a single specimen. The raw mechanical data collected directly from one experiment included the load applied to the sample, the displacement and their variations with time, which were converted into stress versus strain curves and strain rates. The collected mechanical data were corrected for rig distortion, the strength of iron jackets surrounding dolomite specimens, and the cross-sectional area of specimens assuming that the sample volume was constant during deformation. Details regarding the deformation apparatus and data processing can be found in Shao et al. (2011) and Li et al. (2013), respectively.

In most deformation experiments of Fangshan dolomite, a mechanical steady state was not achieved. For specimens deformed at a relatively low temperature (<700°C), the stress versus strain curves show a pronounced hardening behavior without reaching a steady state and strain weakening. In this case, differential stresses at 5% strain were taken as the flow stresses of the specimens. When the total strain for the constant-strain-rate test or one step of the strain-rate-stepping test was less than 5%, the strain hardening after the yield point was fitted by the following power function:

$$\sigma = A \times \left(\varepsilon - b\right)^m$$

where σ and ε are the real-time differential stress and strain, respectively; A, b, and m are fitting parameters. The differential stress at 5% strain can be read from the curve extrapolated by the power function and considered the flow stress. For specimens deformed at a relatively high temperature (>700°C), the stress versus strain curves exhibit a strain weakening behavior after strain hardening. In such a case, the peak differential stresses of the stress-strain curves were taken as the flow stresses prior to recrystallization and strain localization (Holyoke et al., 2014a).

For deformation experiments at high temperatures above ~700°C, dolomite undergoes a dissociation reaction (dolomite → calcite + periclase + CO_2). The released CO_2 gas was sealed in the assembly by the iron jacket and two alumina ceramic spacers without a central hole, and thus, the generated CO_2 could induce pore pressure inside the specimen. As previously mentioned, the porosity of the starting material (Fangshan dolomite) was less than 1%; therefore, reaction equilibrium was likely achieved by dissociation of trace amounts of dolomite at the grain boundaries of the dolomite aggregates. Hence, the stability of the dolomite was maintained in the process of deformation due to the generation of an internal CO_2 pore pressure by dolomite dissociation. These inferences are supported by optical observations and microstructure analysis of the deformed specimens. According to the reaction equilibria of dolomite presented by Goldsmith (1959), equilibrium CO_2 pore pressures at different temperatures could be obtained, and the effective confining pressures could be determined as follows:

$$P_e = P_c - P_{CO_2}$$

where P_e, P_c, and P_{CO_2} represent the effective confining pressure, confining pressure, and pore fluid pressure generated by CO_2, respectively. Most of the deformation experiments in this work were performed under a confining pressure of ~300 MPa; hence, the effective confining pressure varied for experiments at temperatures higher than 700°C when small amounts of dolomite decomposition occurred. As effective confining pressure can affect the flow stress of dolomite (Davis et al., 2008), it is necessary to correct the flow stress of dolomite to the same effective confining pressure (~300 MPa) to accurately establish the flow law of dolomite.

Davis et al. (2008) observed that the flow stress of Madoc dolomite exhibits a linear dependence on the effective confining pressure (which can be described by an apparent coefficient of internal friction of

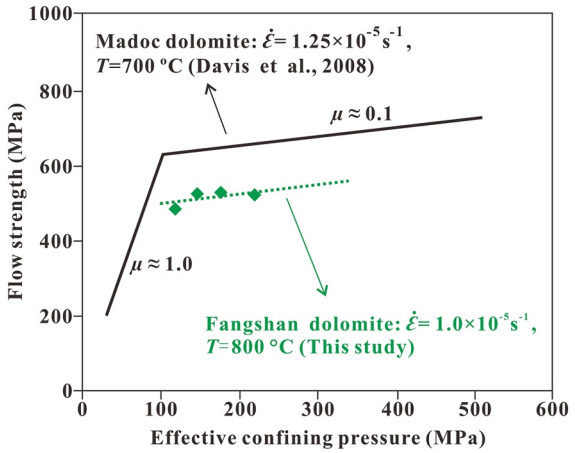

Figure 4. Dependence of flow stress on effective confining pressure (P_e) for polycrystalline dolomite aggregates. Black solid lines are fitting results of coarse-grained Madoc dolomite from Davis et al. (2008). At P_e > 100 MPa, 700°C, and a strain rate of 1.25 × 10^{-5} s^{-1}, the flow stress of Madoc dolomite exhibits a linear dependence on the effective confining pressure with a small apparent coefficient of internal friction of approximately 0.1 ($\mu \cong 0.1$). In contrast, at P_e < 100 MPa, the dependence of the flow stress on the effective confining pressure satisfies the Mohr-Coulomb criterion with an apparent coefficient of internal friction of approximately 1.0 ($\mu \cong 1.0$). Green solid diamonds represent the data of medium-grained Fangshan dolomite deformed at 800°C and 1.0 × 10^{-5} s^{-1}, and the green dotted line is a linear fitting that shows a weak dependence of flow stress on effective pressure with an apparent inner friction coefficient of 0.1.

$\mu \cong 0.1$ when deformed at P_e > 100 MPa, 700°C and a strain rate of 1.25 × 10^{-5} s^{-1}). Such a correlation between flow stress and effective confining pressure was also obtained for Dover Plains dolomite and Hasmark dolomite (Handin & Fairbairn, 1955; Turner et al., 1954). When deformed at P_e < 100 MPa, the differential stress of Madoc dolomite exhibits a linear dependence on the effective confining pressure, which can be described by the Mohr-Coulomb criterion with an apparent coefficient of internal friction of approximately 1.0 ($\mu \cong 1.0$) (Figure 4; Austin & Kennedy, 2005; Austin et al., 2005; Davis et al., 2008). Our experimental results of specimens FS34 and FS26 deformed at P_e > 100 MPa and 800°C and strain rates of 10^{-5} s^{-1} indicate that the flow stress of Fangshan dolomite also exhibits a weak linear dependence on effective confining pressure, which is similar to that of Madoc dolomite. Accordingly, in this study, the flow stress of Fangshan dolomite was corrected to an effective confining pressure of 300 MPa by using empirical correlations between the flow stress and the effective confining pressure. For deformation experiments in which dolomite decomposed (>700°C), if $P_e \geq 100$ MPa, the flow stress was corrected as follows:

$$\sigma_t = \sigma_{5\%} + 0.1 \times \left(300 - P_e\right) \quad (1)$$

where σ_t is the true flow stress at an effective confining pressure of 300 MPa, $\sigma_{5\%}$ is the differential stress at 5% strain, and P_e is the effective confining pressure. If P_e < 100 MPa, the true flow stress was calculated according to:

$$\sigma_t = \sigma_{5\%} + \left(100 - P_e\right) + 0.1 \times \left(300 - 100\right) \quad (2)$$

2.4. Microstructure Observations

Specimens deformed at various strain rates and temperatures were inspected to characterize their deformation microstructures mainly by conventional optical observations using a Leica microscope. The specimens were impregnated with epoxy resin and then cut in half along the direction of the compression axis. Half of the specimen was doubly polished to make ultrathin sections of approximately 10 μm in thickness. Microcracks were judged by optical observations of the thin sections in plane-polarized light. Mechanical twinning, undulating extinctions, deformation bands, and recrystallized grains were observed in cross-polarized light. SEM was also used to characterize the dissociation reaction products and recrystallized grains of dolomite.

3. Results

3.1. Mechanical Data

A total of 32 specimens of Fangshan dolomite were deformed in triaxial compression under constant-strain-rate or strain-rate-stepping conditions. The experimental conditions and mechanical results of the constant-strain-rate experiments are listed in Table 2, and those of the strain-rate-stepping experiments are listed in Table 3. Here, the flow stresses were determined by peak differential stresses and/or differential stresses at 5% strain. Typical differential stress versus strain curves for the constant-strain-rate experiments and the strain-rate-stepping experiments are depicted in Figures 5 and 6, respectively.

Based on an analysis of the mechanical results and the differential stress versus strain curves of Fangshan dolomite, especially the strain rate and temperature dependencies of flow stress, three deformation regimes have been identified: intracrystalline plasticity at low temperature or LTP (≤500°C, Regime 1), dislocation creep at high temperature (≥800°C, Regime 2), and a transitional regime between LTP and dislocation creep (Regime 3). The detailed rheological behavior of these three regimes is described as follows:

Table 2
Test Conditions and Mechanical Results of Constant-Strain Rate Tests

Sample	P_c ① (MPa)	P_e ② (MPa)	T (°C)	$\dot{\varepsilon}$ (s^{-1})	ε_P ③ (%)	σ_P ④ (MPa)	$\sigma_{5\%}$ ⑤ (MPa)	σ ⑥ (MPa)	ε_f ⑦ (MPa)
FS5	300	300	27	1.0×10^{-5}	NA	NA	810.0	810.0	3.1
FS14	300	300	27	1.6×10^{-6}	NA	NA	780.0	780.0	3.7
FS7	300	300	300	1.0×10^{-5}	NA	NA	765.4	765.4	6.4
FS8	300	300	500	7.8×10^{-6}	NA	NA	819.0	819.0	7.0
FS10	300	270	700	1.7×10^{-5}	NA	NA	629.5	632.5	3.5
FS21	300	250	750	1.0×10^{-5}	8.1	642.5		647.5	13.2
FS22	300	250	750	5.0×10^{-6}	7.1	603.7		608.7	11.6
FS23	300	250	750	2.0×10^{-5}	8.1	677.9		682.9	18.0
FS24	300	250	750	4.0×10^{-5}	9.6	705.5		710.5	13.5
FS2	300	220	800	2.5×10^{-5}	5.6	609.1		614.7	7.6
FS25	300	220	800	5.0×10^{-6}	5.9	426.5		434.5	14.1
FS26	300	220	800	2.0×10^{-5}	5.9	519.9		527.9	13.8
FS27	300	220	800	1.0×10^{-5}	5.4	510.0		518.0	14.5
FS28	300	220	800	4.0×10^{-5}	6.8	538.6		546.6	12.7
FS29	300	220	800	1.0×10^{-5}	6.0	423.2		431.2	9.8
FS30	260	60	850	1.0×10^{-5}	4.2	228.5		284.5	17.1
FS31	260	60	850	4.0×10^{-5}	4.4	339.3		395.3	15.1
FS32	260	60	850	2.0×10^{-5}	4.8	287.8		343.8	10.5
FS33	260	60	850	5.0×10^{-6}	5.0	175.1		231.1	9.5
FS1	300	50	900	2.5×10^{-5}	2.8	183.2		253.2	9.0
FS12	300	50	900	2.3×10^{-6}	5.8	90.1		160.1	7.3

① Confining Pressure; ② Effective pressure by assuming $P_e = P_c - P_{CO_2}$; ③ Axial strain at peaks differential stress; ④ Peak differential stress; ⑤ Differential stress at axial strain 5%; ⑥ Flow stress corrected by P_e; ⑦ Axial strain at the end of experiment; NA = not applicable.

Regime 1 (≤500°C). LTP dominates the deformation of Fangshan dolomite at temperatures ≤500°C. Several typical curves of differential stress versus strain collected at 27, 300, and 500°C are given in Figure 5a. Differential stress exhibits a linear relation with strain in the first ~0.5% strain, followed by yielding at stresses ranging between ~350 and 500 MPa, deviating from the linear relationship and exhibiting various degrees of strain hardening (depending on temperature). The differential stress versus strain curves at 27°C (FS5, FS14) exhibit weak strain hardening, whereas those at 300°C (FS7) and 500°C (FS8) exhibit comparable and strong strain hardening behavior. The flow stresses (differential stresses at 5% strain) of Fangshan dolomite deformed at 27, 300, and 500°C are limited to a narrow range between ~765 and 832 MPa (Figure 5a and Tables 2 and 3), indicating that the flow stress has weak dependencies on temperature and strain rate. The weak dependence of flow stress on strain rate can be confirmed further by the results of strain-rate-stepping experiments. Figure 6a presents the differential stress versus strain curves collected from the strain-rate-stepping experiments at 27, 300, and 500°C. It can be seen that increasing or decreasing the strain rate induces a slight increase or decrease in the differential stress. For the curve at 27°C, the flow stress (differential stress at 5% strain) increases from 792 to 813 MPa (21 MPa) when the strain rate increases from 2.1×10^{-6} to 1.5×10^{-5} s^{-1} (~7 times), indicating a very weak sensitivity to the strain rate. To quantify the dependence of flow stress on strain rate and temperature, we plotted the mechanical data into a double logarithmic diagram of differential stress versus strain rate (Figure 7a). The data points at each temperature scatter in a linear trend with high slope values (apparent stress exponent n), which are 78, 71, and 70 for the data collected from the tests at 27°C, 300°C, and 500°C, respectively. The variation in flow stress as temperature increases from room temperature (27°C) to 300°C is negligible; however, when increasing temperature

Table 3
Test Conditions and Mechanical Results of Strain-Rate-Stepping Tests

Sample	P_c [1] (MPa)	P_e [2] (MPa)	T (°C)	$\dot{\varepsilon}$ (s^{-1})	$\sigma_{5\%}$ [3] (MPa)	σ [4] (MPa)	ε_f [5]
FS6	300	300	27	1.0×10^{-5}	807.0	807.0	
				2.1×10^{-6}	792.0	792.0	
				1.0×10^{-5}	807.0	807.0	
				1.5×10^{-5}	813.0	813.0	6.3
FS9	300	300	300	6.6×10^{-6}	804.0	804.0	
				9.3×10^{-7}	787.0	787.0	
				8.5×10^{-6}	803.0	803.0	
				4.2×10^{-6}	796.5	796.5	
				8.9×10^{-7}	777.0	777.0	7.2
FS16	300	300	500	1.8×10^{-6}	819.1	819.1	
				2.3×10^{-5}	832.0	832.0	
FS20	300		600	5.0×10^{-6}	742.2	742.2	
				1.0×10^{-5}	752.8	752.8	9.1
FS11	300	270	700	7.0×10^{-6}	704.0	707.0	
				3.3×10^{-6}	682.0	685.0	
				2.3×10^{-5}	733.1	736.1	9.4
FS18	300	270	700	4.8×10^{-6}	680.0	683.0	
				1.0×10^{-5}	702.0	705.0	
				2.5×10^{-5}	716.0	719.0	
				4.2×10^{-5}	725.3	728.3	
FS13	300	220	800	1.9×10^{-6}	365.0	373.0	
				9.8×10^{-6}	440.3	448.3	7.8
FS15	300	220	800	8.6×10^{-6}	452.7	460.7	
				3.1×10^{-6}	NA		11.1
FS17	300	220	800	8.3×10^{-6}	480.0	488.0	
				5.1×10^{-5}	579.0	587.0	
				8.5×10^{-5}	598.7	606.7	
				1.9×10^{-4}	643.6	651.6	8.8
FS19	300	70	870	1.0×10^{-5}	202.4	252.4	
				2.5×10^{-5}	244.8	294.8	4.1
FS34	257	177	800	1.0×10^{-5}	515.7	523.7	
	227	147	800	1.0×10^{-5}	512.3	520.3	
	199	119	800	1.0×10^{-5}	472.4	480.4	

[1] Confining pressure; [2] Effective pressure by assuming $P_e = P_c - P_{CO_2}$; [3] Differential stress at axial strain 5%; [4] Flow stress corrected by P_e; [5] Axial strain at the end of experiment; NA = not applicable.

from 300°C to 500°C, the flow stress exhibits a slight increase (Figures 7a and 8a), which is unusual because it cannot be described by an Arrhenius relationship.

Regime 2 (≥800°C). Dislocation creep dominates the deformation of Fangshan dolomite at temperatures higher than 800°C or equal to 800°C at a strain rate of ≤~1.0×10^{-5} s^{-1}. The flow stresses in this regime are in the range of 90–510 MPa, and the corrected flow stresses to P_e = 300 MPa are in the range of 160–518 MPa. The differential stress versus strain curves collected from constant-strain-rate experiments at 800°C, 850°C, and 900°C indicate that the differential stress shows yield after a linear elastic deformation, followed by hardening until a peak stress is reached at ~3%–6% strain, and finally exhibits strain weakening before achieving an approximate steady state (Figures 5c and 5d; Table 2). Generally, the peak stress decreases and shifts to lower strain with increasing temperature and decreasing strain rate, and strain weakening is enhanced with increasing temperature (Figures 5c and 5d; Table 2). For example, the peak stresses and onset of strain weakening occur at 5.4%–6.8% strain for the stress-strain curves at T = 800°C (Figure 5c and Table 2), whereas the peak stresses are obtained at 4.2%–5.0% strain for the stress-strain curves at T = 850°C (Figure 5d and Table 2). The peak stress (flow stress) is in a wide range of 423–609 MPa at 800°C and 175–339 MPa at 850°C, exhibiting a much stronger strain rate and temperature dependence than the LTP regime. The strong dependence of flow stress on strain rate can be further confirmed by the strain-rate-stepping experiments, as depicted in Figures 6c and 6d. For example, at 800°C, as the strain rate decreases from 1.9×10^{-4} to 8.3×10^{-6} s^{-1} (1/20), the flow stress decreases from 644 to 480 MPa (164 MPa) (FS17; Table 3 and Figure 6c).

To analyze the mechanical results quantitatively in the dislocation creep regime, the corrected flow stress versus strain rate data are plotted in a double logarithmic diagram (Figure 7c). The flow stresses from the constant-strain-rate experiments (peak differential stresses) are consistent with those from the strain-rate-stepping experiments (differential stresses at 5% strain), although some scatter in the data is apparent (Figures 5c and 6c). The linear relationship between the strain rate and flow stress has a slope (stress exponent value) of 3.8–5.4 (Figure 7c), which is consistent with the expected values of the stress exponent for dislocation creep. As the temperature in this regime increases or decreases, the flow stresses decrease or increase systematically (Figures 7c and 8a). In the diagram of logarithmic flow stress versus 1,000/T (Figure 8b), a significant positive linear relationship with a steeply inclined slope ($\rho = \frac{Q * \log e}{nR} = 4.82 - 4.86$ in Figure 8b) is found at high temperature (≥800°C), which is obviously different from the approximately horizontal negative slope at temperatures lower than 500°C.

Regime 3 (500°C < T ≤ 800°C). This regime refers to a transitional deformation regime between LTP (Regime 1) and dislocation creep (Regime 2), which is predominant at temperatures between 500°C and 800°C. The differential stress versus strain curves from the constant-strain-rate experiments (Figure 5b) are similar to those of dislocation creep (Figures 5c and 5d), but the strain weakening is less significant and occurs at higher strains of 7%–10%. The dependence of the flow stress on strain rate in the transitional regime is stronger than that in the LTP regime (Regime 1) but weaker than that in dislocation creep (Regime 2), as indicated by the strain-rate-stepping experiments (Figure 6 and Table 3) and the apparent stress exponent values in the range of 11.3–48.7 (Figure 7b). The transitional deformation state

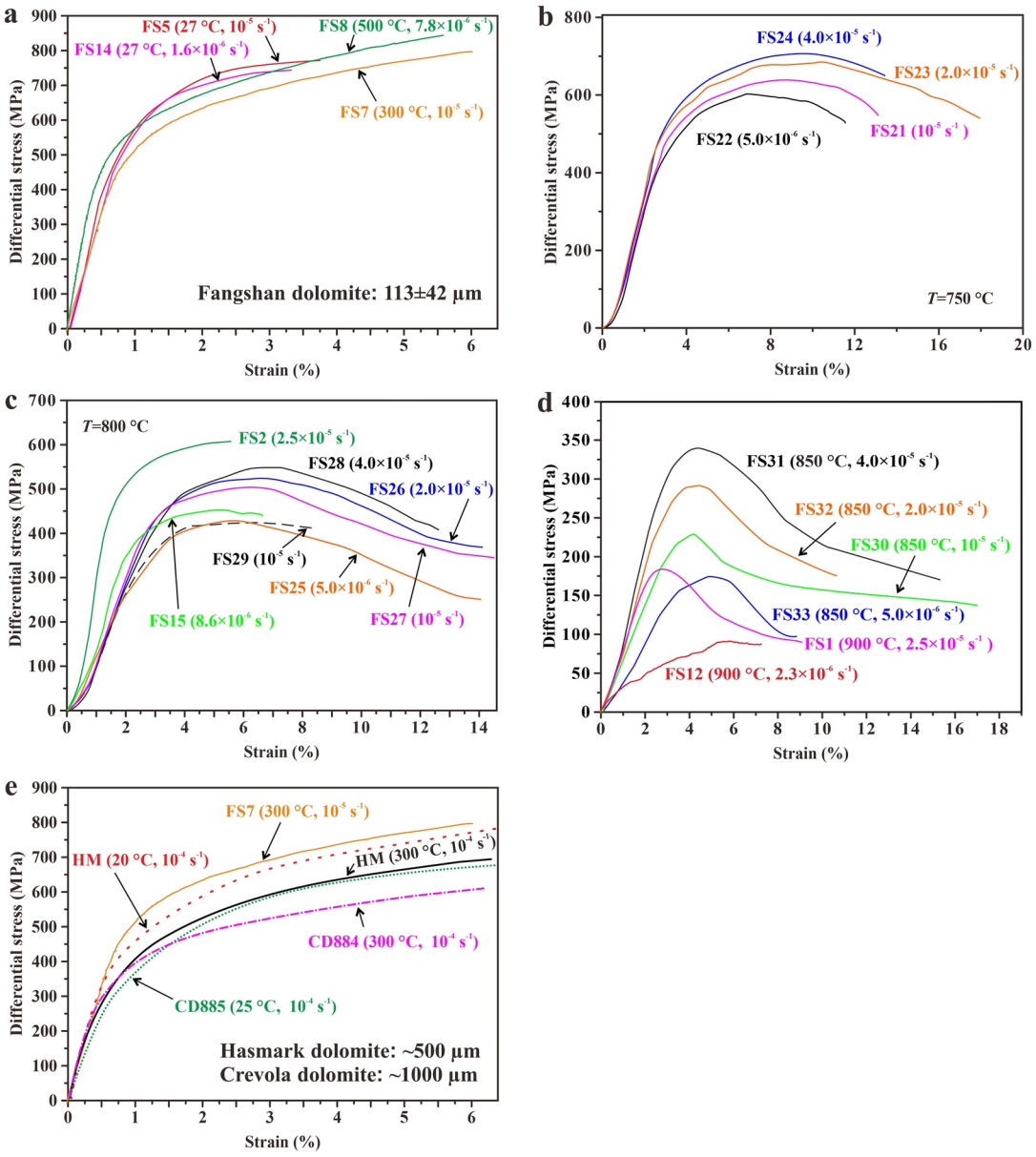

Figure 5. Differential stress versus strain curves of Fangshan dolomite from the constant-strain-rate experiments: (a) 27°C–500°C, (b) 750°C, (c) 800°C, and (d) 850°C–900°C. Previous results for Hasmark dolomite (HM; Handin & Fairbairn, 1955), Crevola dolomite (CD; Barber et al., 1994), and Madoc dolomite (MD; Davis et al., 2008), which were obtained at a strain rate of 10^{-4} s^{-1}, are presented in Figure 5e for comparison. The effective confining pressures for all our tests on Fangshan dolomite are in the range of 50–300 MPa. The respective sample name or number (FS denotes Fangshan dolomite), strain rate and temperature are marked for each curve.

for Fangshan dolomite can also be recognized by the dependence of flow stress on temperature (Figure 8a), which is intermediate to the temperature-insensitive deformation at lower temperatures (<500°C) and the strong temperature dependence of deformation at higher temperatures (≥800°C).

In general, Fangshan dolomite deformed in the dislocation creep regime exhibits lower flow stress and stronger dependencies of flow stress on temperature and strain rate than in the LTP regime. In addition, the dependence of flow stress on temperature is negative in dislocation creep, whereas it is weakly positive in the LTP regime.

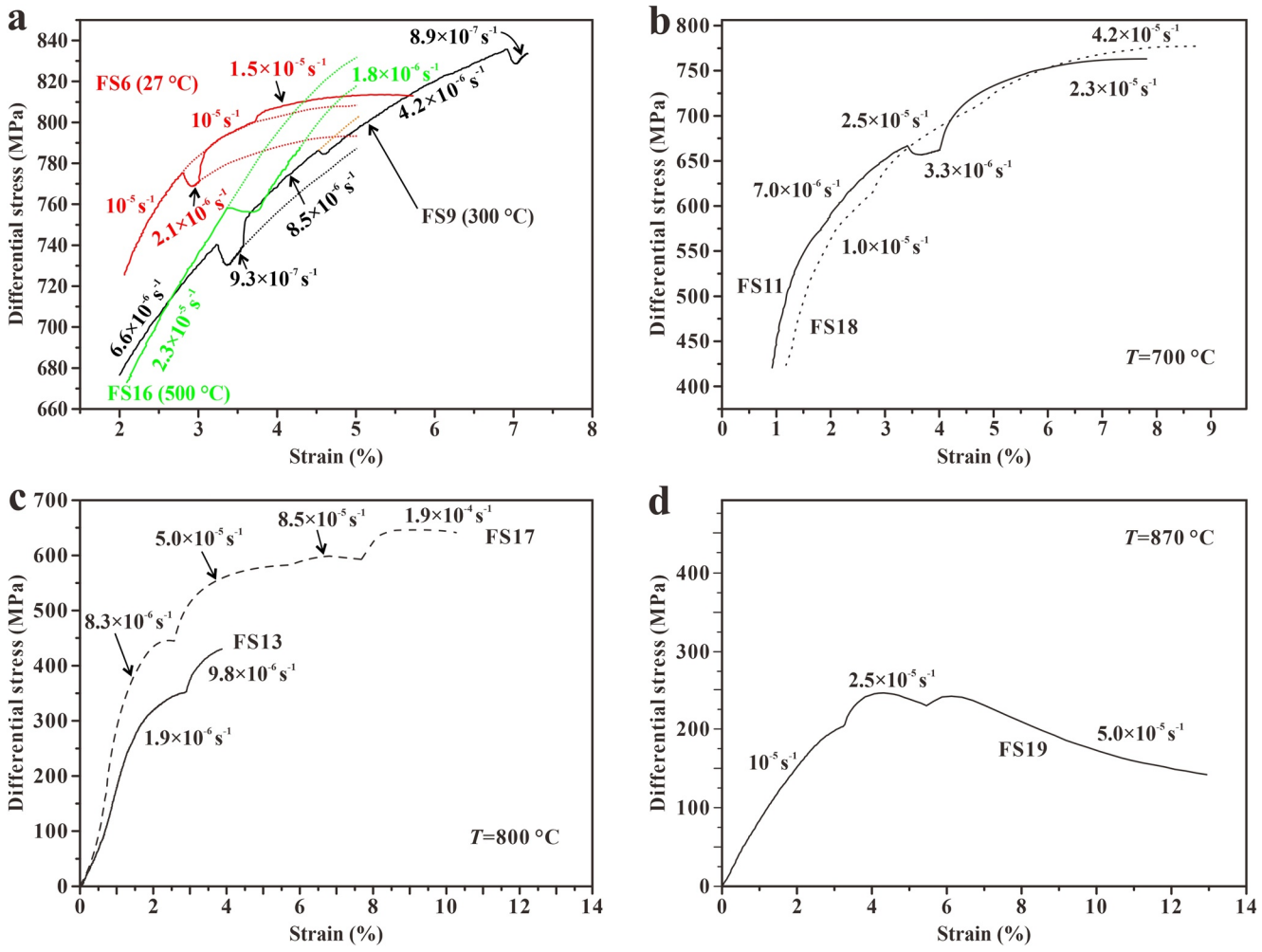

Figure 6. Differential stress versus strain curves of Fangshan dolomite from the strain-rate-stepping experiments: (a) 27°C–500°C, (b) 700°C, (c) 800°C, and (d) 870°C. The sample names are marked for each curve, and the strain rates are marked for each step of the curves. In Figure 6a, curves of different specimens (temperature) are presented in different colors and the dotted lines represent the extrapolations of strain-rate steps to calculate the differential stresses at 5% strain.

3.2. Microstructures

The deformation microstructures of Fangshan dolomite at the optical and SEM scales are described and distinguished briefly for the three deformation regimes by mechanical behavior.

(1) Specimens deformed in Regime 1 (≤500°C)

Optical observations reveal that the microstructures of the specimens deformed in the LTP regime are characterized by abrupt undulatory extinctions and/or a preponderance of mechanical twins. The specimens deformed at room temperature (27°C) display undulatory extinctions and a small number of mechanical twins (Figures 9a and 9b). The population of mechanical twins is much higher in the specimens deformed at 300°C than in those deformed at room temperature (Figures 9c and 9d), and is the most abundant in the specimens deformed at 500°C (Figures 9e and 9f). In addition to mechanical twins, undulatory extinction was also observed in some dolomite grains of the specimens deformed at 300°C and 500°C (Figures 9b and 9d). The mechanical twins formed during deformation were usually lensoidal in shape, with tapering ends close to or at the grain boundaries. The characteristic shape of mechanical twin lamellae makes them easily distinguishable from the straight boundaries of the twin lamellae that either exist in the starting material or are produced by the quenching process at the end of the experiment. In addition, despite the high flow stresses at temperatures ≤500°C, which are much higher than the confining pressure, brittle

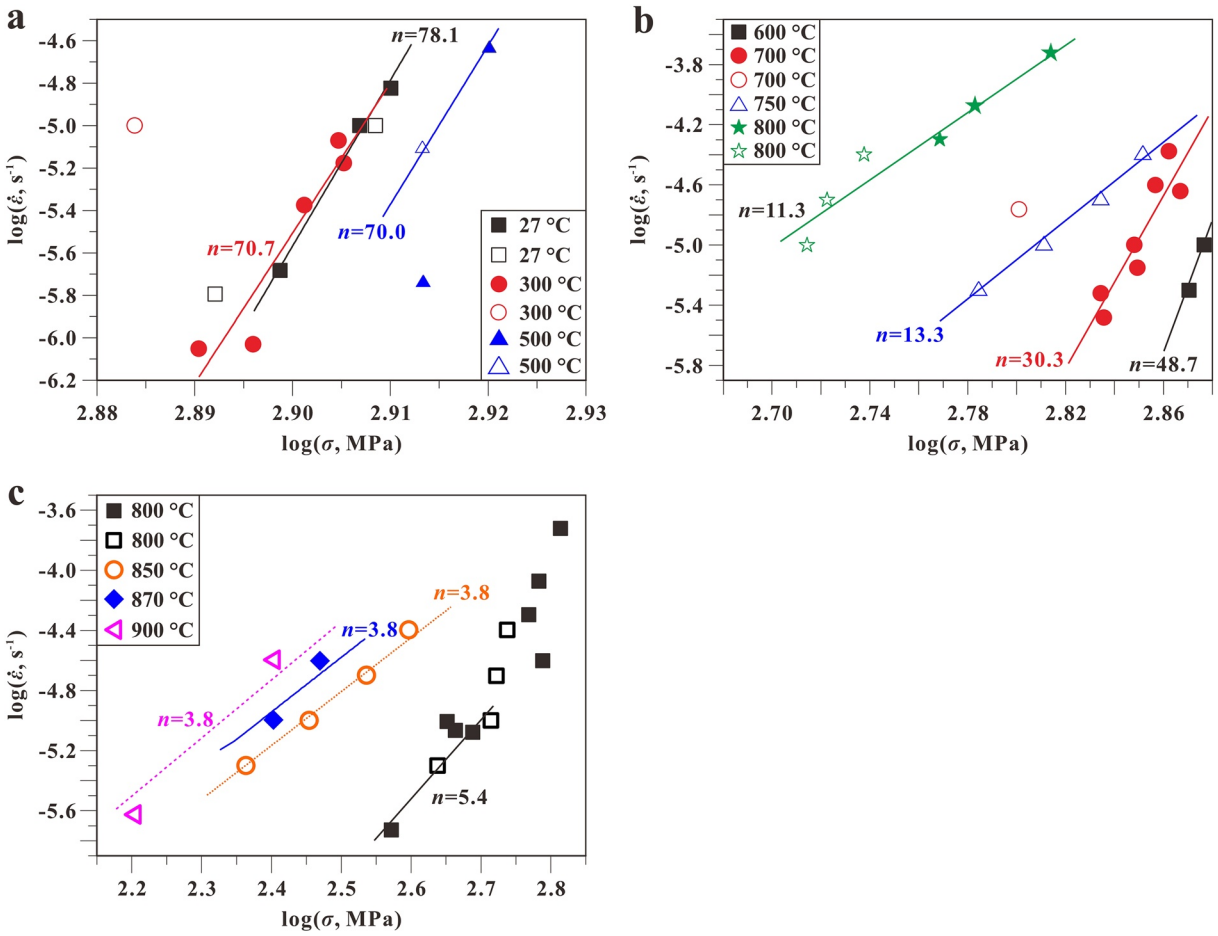

Figure 7. log $\dot{\varepsilon}$ versus log σ plots for Fangshan dolomite deformed in (a) LTP, (b) transitional, and (c) dislocation creep regimes. All mechanical data are collected from deformation experiments at a confining pressure of 300 MPa, and all the flow stresses are corrected to an effective confining of 300 MPa. The LTP regime at temperatures ≤500°C has extremely high values of the stress exponent (n = ~70), implying weak dependence of the flow stress on the strain rate. The transitional regime at temperatures from 600°C to 800°C has moderate values of the stress exponent, which gradually decrease with increasing temperature (the n value decreases from 48.7 at 600°C to 13.3 at 750°C). The dislocation creep regime at temperatures of 800°C and higher is characterized by low values of the stress exponent (3.8–5.4), which are consistent with typical values of n = 3–5 expected for dislocation creep. The solid and open symbols denote data collected from the strain-rate-stepping experiments and the constant-strain-rate experiments, respectively. LTP, low-temperature plasticity.

deformation processes are not very apparent, with microcrack densities that are not substantially greater than those found in the starting material.

(2) Specimens deformed in Regime 2 (≥800°C)

The specimens deformed at temperatures ≥800°C have smooth undulatory extinctions and similar densities of twins to the starting material (Figures 10a and 10b). In addition, limited numbers of recrystallized fine grains and some subgrains exist, mainly at triple junctions and along the grain boundaries of the dolomite grains (Figures 10c and 10d). In the SEM images, fine grains with an equiaxed polygonal shape are distributed along the boundaries of some coarse original dolomite grains (Figures 10g and 10h). These fine grains formed by dynamic recrystallization to accommodate dislocation creep. There are also fine grains surrounding the dolomite grains (Figures 10d and 10e) and accessory minerals such as mica (Figure 10f). EMPA results indicate that some of these grains are high Mg calcite (Table 4), as one of the reaction products of dolomite dissociation, much as observed by Delle Piane et al. (2008). In Figure 10d, reaction products composed of very fine grains are adjacent to the recrystallized fine grains, which are adjacent to the coarse dolomite grains.

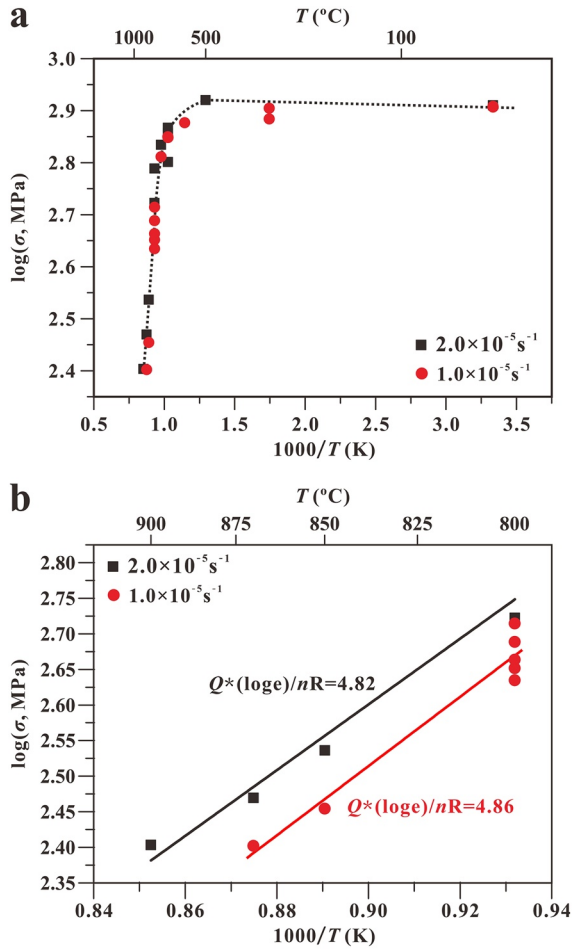

Figure 8. logσ versus 1,000/T plots for Fangshan dolomite displaying the variation in flow stress as a function of temperature. (a) Flow stresses of Fangshan dolomite are not sensitive to temperature variations at low temperature (≤500°C), where the flow stresses exhibit a slight increase with increasing temperature, but are strongly dependent on temperature at high temperature (≥800°C), which clearly indicates two end-member deformation regimes (LTP and dislocation creep) and a transitional regime at temperature of 500°C < T ≤ 800°C. (b) For 800°C ≤ T ≤ 900°C, fitting the logσ versus 1,000/T relationship yields two close values of slope Q*(loge)/nR = 4.86 for data at a strain rate of 1×10^{-5} s^{-1} and Q*(loge)/nR = 4.82 for data at 2×10^{-5} s^{-1}. The solid circles and squares denote data at strain rates of 1×10^{-5} s^{-1} and 2×10^{-5} s^{-1}, respectively. LTP, low-temperature plasticity.

(3) Specimens deformed in Regime 3 (~500°C < T ≤ 800°C)

The specimens deformed at temperatures from 500 to 800°C have transitional microstructures that can be compared with those deformed in Regime 1 to Regime 2. Hence, the specimens deformed at relatively low temperatures of 600°C and 700°C have a greater number of mechanical twins and are similar to those deformed in the LTP regime; the specimens deformed at relatively high temperatures of 750 and 800°C have microstructures similar to those deformed in the dislocation creep regime with the exception that they lack fine grains generated by dolomite dissociation.

4. Discussion

4.1. Strength Comparison With Other Dolomites in LTP and Dislocation Creep

When deformed by LTP, the medium-grained (113 ± 42 μm) Fangshan dolomite is much stronger than the coarse-grained Hasmark, Madoc, or Crevola dolomites (Figure 5e and Table 5). In addition, the fact that coarse materials have lower strength was applied not only between the medium-grained Fangshan dolomite and the coarse-grained (~500 μm) Hasmark or Crevola dolomite but also between the latter two coarse-grained dolomites (cf., HM and CD884 in Figure 5e). In contrast, when deformed by dislocation creep at high temperatures ≥800°C, the medium-grained Fangshan dolomite was much softer than the coarse-grained Madoc dolomite. For example, the strength of the Fangshan dolomite was 253.15 MPa at 2.5×10^{-5} s^{-1} and 900°C (FS1), which is ~100 MPa lower than the strength of the Madoc dolomite of 370 MPa at 1.0×10^{-5} s^{-1} and 900°C (D-17 of Holyoke et al. (2013), Table 5). This strength contrast among different dolomites may result from grain boundary effects in different deformation regimes; hence, the denser grain boundaries in fine-grained dolomite hinder dislocation slip/glide in the LTP regime but promote dislocation climb in the dislocation creep regime.

At low temperatures of ≤300°C, both Hasmark dolomite (Handin & Fairbairn, 1955) and Crevola dolomite (Barber et al., 1994) exhibit flow stresses that slightly increase with decreasing temperature (Figure 5e). The same is true for our Fangshan dolomite deformed at temperatures ≤300°C and strains <~5%, where at the same strain rate of 10^{-5} s^{-1}, sample FS5 (deformed at room temperature) is stronger than sample FS7 (deformed at 300°C) (Figure 5a). This is also true for samples compressed at temperatures ≥500°C. For instance, the flow stress of sample FS8 (deformed at 500°C and 7.8×10^{-6} s^{-1}) is much higher than that of sample FS10 (deformed at 700°C and 1.7×10^{-5} s^{-1}) (Table 2). From 300°C to 500°C, however, an unusual increase in the flow stress of Fangshan dolomite occurs with increasing temperature (Figure 5a), which is similar to the temperature dependence of the flow stress of coarse-grained Madoc at temperatures ≤700°C (see Figure 2b from Davis et al., 2008).

4.2. Deformation Mechanisms of Fangshan Dolomite

There have been a number of experimental studies on the rheological properties of dolomite, although a far greater number of such studies have investigated calcite. Early experimental studies of dolomite deformation are limited to a restricted set of conditions and were performed, mostly at relatively low temperatures (<500°C) (e.g., Barber et al., 1994; Handin & Fairbairn, 1955; Turner et al., 1954). Some deformation experiments on dolomite single crystals were performed at high temperature (1,000°C); these experiments

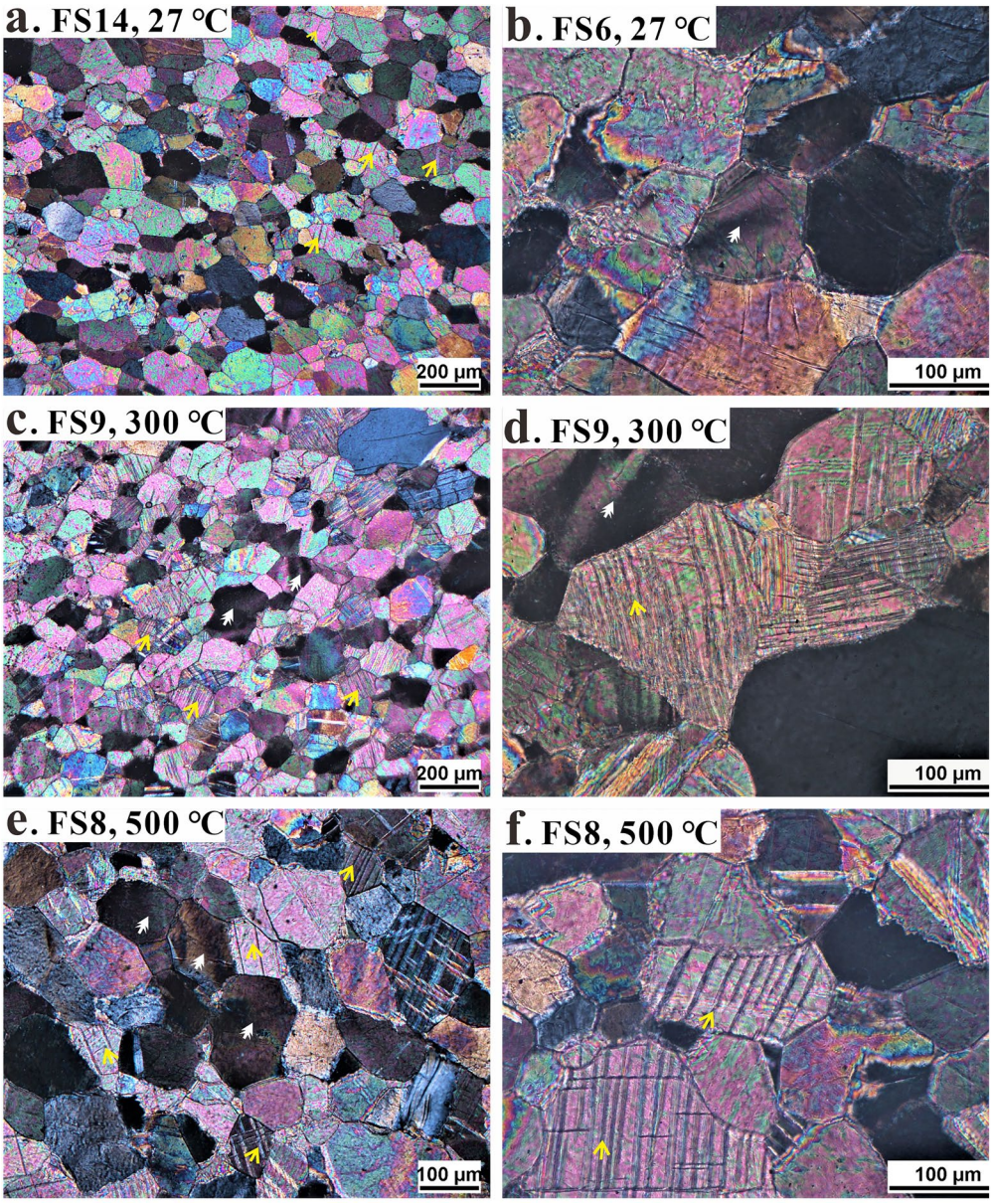

Figure 9. Optical microstructures of Fangshan dolomite specimens deformed at temperatures ≤500°C in cross-polarized light. (a and b) Undulatory extinction and extinction bands developed in the Fangshan dolomite deformed at room temperature (FS14, 27°C, 1.6×10^{-6} s^{-1}, total strain $\varepsilon = 3.7\%$; FS6, 27°C, stepping strain rates 1.5×10^{-5} to 2.1×10^{-6} s^{-1}, $\varepsilon = 6.3\%$). (c and d) Both undulatory extinction and f-twins were pervasive in a specimen deformed at 300°C (FS9, 300°C, stepping strain rates 8.5×10^{-5} to 8.9×10^{-6} s^{-1}, $\varepsilon = 7.2\%$). (e and f) f-Twinning became dominant in the Fangshan dolomites at 500°C (FS8, 500°C, 7.8×10^{-6} s^{-1}, $\varepsilon = 7.0\%$). Undulatory extinction is marked by white arrows, whereas the mechanical twins are marked by yellow arrows.

offer microstructural evidence of dislocations generated within grains (Barber et al., 1981, 1983). Deformation microstructures were reported by Neumann (1969) but poor stress resolution of early solid-medium experimental methods precludes determinations of flow laws. In recent years, the rheological properties of dolomite have been systematically investigated over a wide range of temperatures, pressures and strain rates using deformation apparatuses with high stress resolution, including Heard-type and Paterson gas-medium apparatuses (Davis et al., 2008; Delle Piane et al., 2008) and Griggs apparatus with low strength solid medium and molten salt cells (Holyoke et al., 2013). From these studies, three regimes of deformation—LTP, dislocation creep and diffusion creep—are distinguished, and the corresponding flow laws are reported.

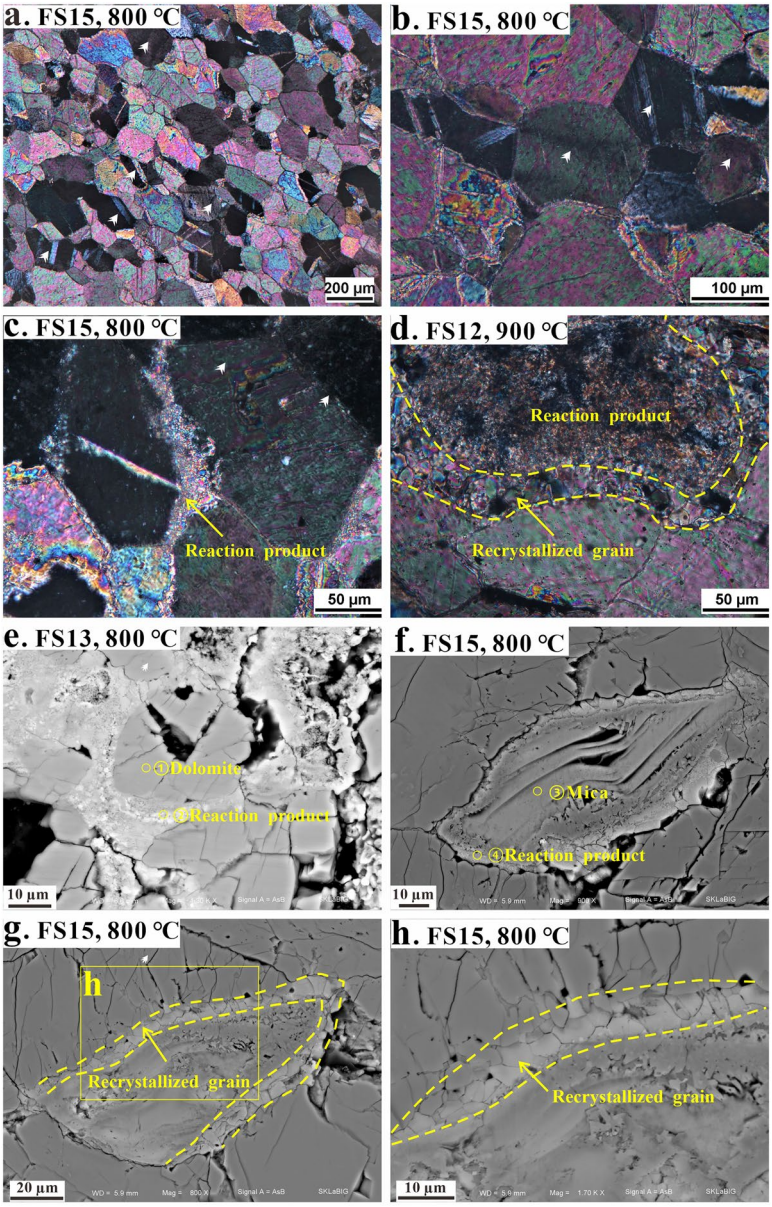

Figure 10. (a–d) Cross-polarized light and (e–h) SEM images showing microstructures of Fangshan dolomite deformed at temperatures ≥800°C. (a and b) Smooth undulating extinctions in the Fangshan dolomites deformed at 800°C (FS15, 800°C, stepping strain rates, $\varepsilon = 11.1\%$). (c and d) New fine grains at the triple junction and boundaries of dolomite grains are formed by recrystallization and dissociation of dolomite (FS15, 800°C, stepping strain rates, $\varepsilon = 11.1\%$; FS12, 900°C, 1.6×10^{-6} s^{-1}, $\varepsilon = 7.3\%$). (e and f) Reaction products of dolomite dissociation around original coarse dolomite grains and mica (FS13, 800°C, stepping strain rates, $\varepsilon = 7.8\%$; FS15, 800°C, stepping strain rates, $\varepsilon = 11.1\%$). (g and h) Fine grains are formed by recrystallization during deformation. As shown in (d), fine grains of reaction products are adjacent to the recrystallized grains, which are adjacent to the original coarse dolomite grains. Undulatory extinction is marked by white arrows.

In the diagram of logarithmic stress (logσ) versus reciprocal temperature (1,000/T) (Figure 8a), the flow stress of Fangshan dolomite is not sensitive to temperature with a small negative slope at temperatures between 27°C and 500°C but becomes strongly dependent on temperature with a steep positive slope at temperatures between 800°C and 900°C. This temperature dependence of flow stress for Fangshan dolomite is quite similar to that for Madoc dolomite, even though the temperature insensitivity of flow stress for coarse-grained Madoc dolomite extends up to 700°C (Davis et al., 2008; Holyoke et al., 2013), approximately 200°C

Table 4
Chemical Composition of Four Areas Shown in Figures 10e and 10f Determined by EMPA

Element	①	②	③	④
Al_2O_3	0.009	0.622	15.384	0.479
Na_2O	0.134	0.540	0.138	0.218
K_2O	0.048	0.384	10.715	0.071
Cr_2O_3	0.004	0.035	–	0.051
SiO_2	0.030	0.050	39.451	0.025
MgO	20.338	8.766	23.632	9.783
CaO	29.523	43.357	0.037	48.426
MnO	–	0.074	0.007	0.048
TiO_2	0.016	–	0.628	0.007
FeO	0.104	0.023	0.140	0.112
NiO	0.027	0.010	0.101	–
Total	50.233	53.861	90.233	59.220

higher than that for Fangshan dolomite. Therefore, the field of dislocation creep of Fangshan dolomite is larger than that found for Madoc dolomite at the same pressures (Davis et al., 2008; Delle Piane et al., 2008), with transitional behavior from LTP to dislocation creep shifting to lower temperatures.

Each of the three deformation regimes for Fangshan dolomite exhibits a different dependence of flow stress on strain rate, which is quantitatively expressed by the stress exponent n, choosing a power law to fit the data for all three regimes (Figure 11). The exponential LTP flow regimes at temperatures of 27°C–500°C can be fit by high stress exponent values of 70–78, indicating a weak dependence of flow stress on strain rate and temperature. The dislocation creep regime at temperatures of 800°C–900°C is characterized by low stress exponent values of 3.8–5.4, indicating a stronger dependence of the flow stress to the strain rate, consistent with stress exponent values of $3 \leq n \leq 5$ for dislocation creep (Poirier, 1985). The transitional regime at temperatures of $500 < T \leq 800$°C has intermediate stress exponent values between those in the LTP and dislocation creep regimes and a gradual decrease in the stress exponent value with respect to temperature. The mechanical results of Madoc dolomite are also plotted in Figure 11 for comparison. Using the Madoc dolomite data (Davis et al., 2008), we calculate effective stress exponent values of $n = 53.1 \pm 13.9$ at 600°C, 38.1 ± 7.1 at 700°C, and 24.7 ± 3.8 at 800°C, which fall in the field of the transitional regime. The variation in the stress exponent with respect to temperature for Fangshan dolomite generally agrees well with that for Madoc dolomite (see Figure 11). However, the temperature at which dislocation creep becomes important for Madoc dolomite is higher than that for Fangshan dolomite, as the stress exponent value of 24.7 ± 3.8 at 800°C for Madoc dolomite is still in the transitional regime. These differences may be due to the grain sizes of the Madoc and Fangshan dolomites.

High apparent stress exponent values of 70–78 for the LTP regime at temperatures ≤500°C indicate that dolomite aggregates are deformed by intracrystalline plasticity mechanisms. The specimens of Fangshan dolomite deformed in the LTP regime are characterized by abrupt undulatory extinction and mechanical twins. In particular, mechanical twins are more extensively developed in the specimens deformed at temperatures of 300 and 500°C than in those deformed at room temperature. These microstructural features suggest the simultaneous operation of mechanical twinning and dislocation slip inside the dolomite grains. According to the critical resolved shear stresses (CRSS) for intracrystalline deformation mechanisms (Figure 12; Barber et al., 1981; Higgs & Handin, 1959), we infer that *f*-twinning and *c*-slip are the dominant deformation mechanisms for the LTP regime of Fangshan dolomite.

The specimens deformed in the dislocation creep regime at temperatures ≥800°C are characterized by microstructures including smooth undulatory extinction, mechanical twins (*f*-twins), limited fine recrystallized grains and dolomite dissociation products. The twin densities in these specimens are similar to those of the starting materials, and dolomite recrystallization and dissociation are limited to grain boundaries

Table 5
Differential Stress Comparison Between the Fanshan Dolomite and Other Dolomite Aggregates

Dolomite aggregate		Deformation conditions					
Name	Grain size (μm)	Temperature (°C)	Strain rate (s^{-1})	Yield stress (MPa)	Flow stress (MPa)	Deformation regime	Reference
Fangshan dolomite	113 ± 42	300	10^{-6} to 10^{-5}	352–369	765–804	LTP	This study
Hasmark dolomite	~500	300	1.7×10^{-4}	364	660		Handin and Fairbairn (1955)
Fangshan dolomite	113 ± 42	900	2.5×10^{-5}		253.15	Dislocation creep	This study
Madoc dolomite	240 ± 30	900	1.0×10^{-5}		370		Holyoke et al. (2013)

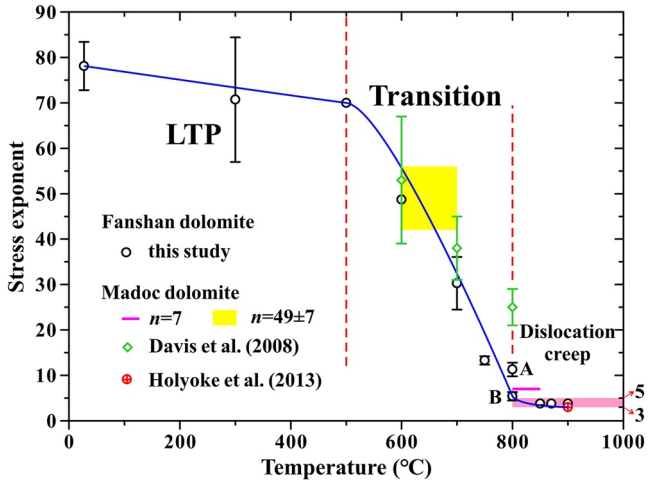

Figure 11. Variation in the stress exponent with respect to temperature for dolomite aggregates. Three distinct deformation regimes—LTP ($T \leq 500$°C), dislocation creep ($T \geq 800$°C) and a transitional regime between LTP and dislocation creep (500°C < $T \leq 800$°C)—can be distinguished clearly for Fangshan dolomite by the values and temperature dependencies of the stress exponent. The black open circles denote data from this study, and the two data points marked by A and B are the stress exponents obtained by fitting the high strain rate ($>\sim10^{-5}$ s^{-1}) and low strain rate ($\leq\sim10^{-5}$ s^{-1}) data at 800°C, respectively (Figures 7b and 7c). The green open diamonds denote the data for Madoc dolomite calculated by fitting the mechanical data at 600°C, 700°C, and 800°C in Figure 5b from Davis et al. (2008). The red open circle denotes the stress exponent $n = 3 \pm 0.1$ for Madoc dolomite at 900°C from Holyoke et al. (2013). The stress exponent $n = 7$ is the value assumed for dislocation creep of Madoc dolomite at 800–850°C by Davis et al. (2008). The stress exponent $n = 49 \pm 7$ is the value of Madoc dolomite at 600–700°C shown in Figure 5b from Davis et al. (2008). LTP, low-temperature plasticity.

and triple junctions. The microstructural features of the dislocation creep regime suggest that recovery processes such as dislocation climb were the most prominent deformation mechanisms, whereas other deformation mechanisms such as mechanical twinning and dynamical recrystallization were also in operation. The significant dependence of stress on the strain rate ($n = 3.8$–5.4) and temperature for the dislocation regime also supports the assertion that dislocation climb dominates the deformation of the dolomite aggregates (Poirier, 1985). According to the CRSS results for experimentally deformed single crystals of dolomite (Figure 12), dislocation slip in the dislocation creep regime should be dominated by *f*-slip, as it has a lower value of CRSS than *c*-slip. The dependence of flow stress on temperature for the dislocation creep regime is much more significant than the dependence of CRSS of *f*-slip on temperature (Figures 8b and 12), further confirming that recovery processes should play an important role in the dislocation creep regime. In addition, dolomite dissociation and dynamic recrystallization, both of which can lead to the generation of fine-grained materials and hence induce diffusion creep, are inferred to be the reasons for strain weakening observed in the differential stress versus strain curves for the dislocation creep regime (e.g., Holyoke et al., 2014b).

4.3. Flow Laws for Fangshan Dolomite

In the LTP regime, the deformation of the dolomite aggregates exhibits weak dependencies of flow stress on strain rate and temperature. In particular, the flow stress unusually increases slightly with respect to temperature, which is inconsistent with thermally activated deformation processes and cannot be described by the Arrhenius relationship (Davies et al., 2008). To describe the flow stresses of the dolomite aggregates in the LTP regime, an exponential flow law without the Arrhenius factor is employed.

$$\dot{\varepsilon} = \dot{\varepsilon}_0 \times \exp\left(\alpha \times \sigma_{5\%}\right) \tag{3}$$

where $\dot{\varepsilon}$ is the strain rate, $\dot{\varepsilon}_0$ is the preexponential term in units of the strain rate (s^{-1}), $\sigma_{5\%}$ is the differential stress at 5% strain, and α (MPa^{-1}) is the fitting parameter. As shown in Figure 13, least square fitting of the mechanical data of Fangshan dolomite at room temperature and 300°C by Equation 3 yields values of $\alpha = 0.0806 \pm 0.0078$ and $\ln\dot{\varepsilon}_0 = -76.66 \pm 6.24$. Fitting of the mechanical data at 500°C yields $\alpha = 0.0836$ and $\ln\dot{\varepsilon}_0 = -80.23$, which is almost the same as the results at room temperature and 300°C. The fitting results agree very well with those for coarse-grained Madoc dolomite ($\alpha = 0.079 \pm 0.010$, $\ln\dot{\varepsilon}_0 = -27.1$, Table 6), and the difference in $\ln\dot{\varepsilon}_0$ is probably due to the difference in grain size between Fangshan dolomite and Madoc dolomite.

The dolomite aggregates deformed in the dislocation creep regime at temperatures ≥800°C exhibit significant dependencies of the flow stress on the strain rate and temperature. The deformation behavior in this regime can be described by a power law equation with an Arrhenius term as follows:

$$\dot{\varepsilon} = A \times \sigma^n \exp\left(\frac{-Q}{RT}\right) \tag{4}$$

where $\dot{\varepsilon}$ is the strain rate, A is a preexponential term, R is the gas constant, Q is the activation energy, T is the absolute temperature in K, n is the stress exponent, and σ is the differential stress (flow stress). The mechanical results of Fangshan dolomite collected at 800°C–900°C, excluding those with flow stresses higher than 520 MPa (or strain rates larger than 1.0×10^{-5} s^{-1}) for the deformation experiments at 800°C, which are in the transitional regime (Figure 7c), were analyzed by Equation 4 to derive the flow law

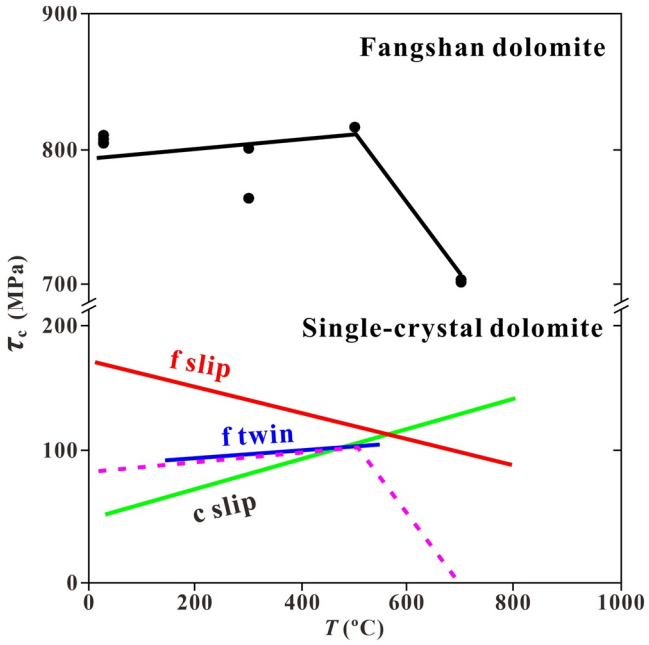

Figure 12. CRSS (τ_c) for dominant slip and twin systems in single-crystal dolomite (Barber et al., 1981). The flow stress data for Fangshan dolomite (denoted as solid circles) are also plotted in the figure for comparison, and the black solid lines show the trend of flow stress variations with respect to temperature. The pink dashed lines are the translation of the black solid lines. The temperature dependence of the flow stress for Fangshan dolomite suggests a transition from deformation dominated by c-slip and f-twinning below 500°C to deformation dominated by f-slip and dislocation creep above 700°C. CRSS, critical resolved shear stresses.

parameters Q and n in the dislocation creep regime. The flow stresses used in the data analysis were those corrected to an effective confining pressure of P_e = 300 MPa (Tables 2 and 3). A least square global fitting of the mechanical results by Equation 4 indicates that the stress exponent $n = 4.75 \pm 0.58$, the activation energy $Q = 436 \pm 54$ kJ/mol and the preexponential term $\log A = 3.48 \pm 1.41$ for Fangshan dolomite in the dislocation regime (Table 6).

4.4. Flow Law Comparison With Madoc Dolomite in Dislocation Creep

Previous experimental studies of dislocation creep of coarse-grained Madoc dolomite (240 ± 30 μm) at high temperatures (>700°C) using gas-medium Heard-type and modified Griggs-type apparatuses (Davis et al., 2008; Holyoke et al., 2013) led to very different flow law parameters Q and n (Table 6). Triaxial compression experiments of Davis et al. (2008) at temperatures of 450–850°C and effective pressures of 200–300 MPa using a gas-medium Heard deformation apparatus with high stress resolution revealed a transition in rheology between LTP and the onset of dislocation creep between 700°C and 800°C. Based on the mechanical data collected at 800°C–850°C, they calculated the parameter ratio of Q/n (=60 ± 5 kJ/mol). Adopting a stress exponent n = ~7, similar to that of dislocation creep of calcite marble (Schmid et al., 1980), they inferred an activation energy Q for dislocation creep of ~410 kJ/mol. However, deformation of Madoc dolomite at 800°C is near the boundary between dislocation creep and LTP of Madoc dolomite, and the mechanical results may represent deformation by both dislocation creep and LTP, as indicated by the apparent stress exponent value of $n = 26 \pm 5$.

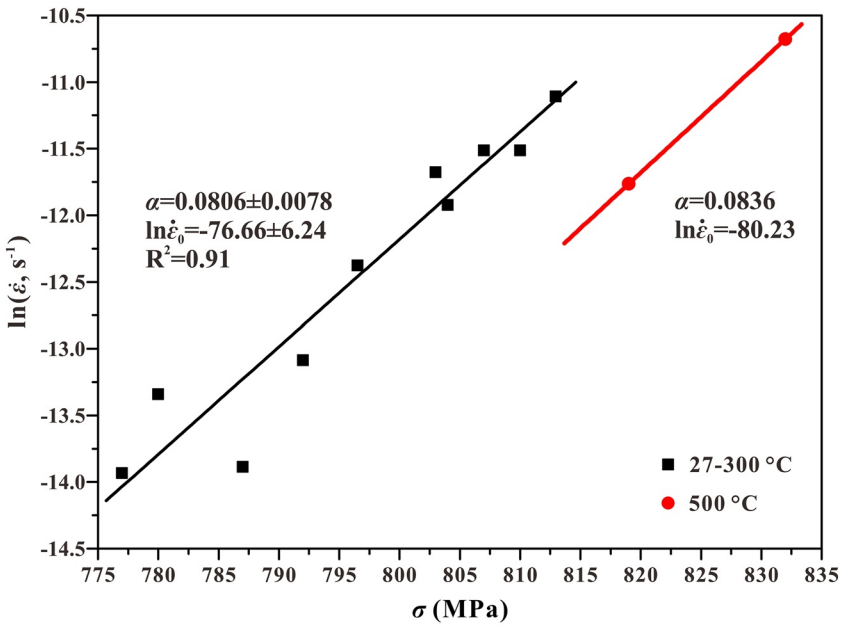

Figure 13. $\log \dot{\varepsilon}$ versus σ plots for Fangshan dolomites deformed in the LTP regime at temperatures ≤500°C. The solid lines are fitting results by Equation 3. The values of the exponential law obtained by fitting the mechanical data at 27°C–300°C are very similar to those obtained by fitting the mechanical data at 500°C. LTP, low-temperature plasticity.

Table 6
Flow Law Parameters of Dolomites

Flow law	α or n	Q or Q/n	Preexponential term	Deformation regime	Dolomite aggregate	Reference
$\dot{\varepsilon} = \dot{\varepsilon}_0 \times \exp(\alpha \times \sigma_{5\%})$	$\alpha = 0.0806 \pm 0.078$		$\ln \dot{\varepsilon}_0 = -76.66 \pm 6.24$	LTP	Fangshan dolomite	This study
	$\alpha = 0.079 \pm 0.01$			LTP	Madoc dolomite	Davis et al. (2008)
$\dot{\varepsilon} = A \times \sigma^n \exp\left(\frac{-Q}{RT}\right)$	$n = 4.75 \pm 0.58$	$Q = 436 \pm 54$ kJ/mol	$\log A = 3.48 \pm 1.41$	Dislocation creep	Fangshan dolomite	This study
	$n = 7$ supposed	$Q/n = 60 \pm 6$ kJ/mol		Dislocation creep	Madoc dolomite	Davis et al. (2008)
	$n = 3.0 \pm 0.1$	$Q = 145 \pm 20$ kJ/mol		Dislocation creep	Madoc dolomite	Holyoke et al. (2013)
$\dot{\varepsilon} = A \times \sigma^n \exp\left(\frac{-Q}{RT}\right)$	$n = 1.28 \pm 0.15$	$Q = 280 \pm 45$ kJ/mol		Diffusion creep		Davis et al. (2008)
	$n = 1.3 \pm 0.2$	$Q = 368 \pm 25$ kJ/mol		Diffusion creep		Delle Piane et al. (2008)

The experimental study of Holyoke et al. (2013) extended the study of dislocation creep of Davis et al. (2008) to temperatures between 700 and 1,000°C and led to a much smaller stress exponent than anticipated by Davis et al. (2008) and a much lower value of the activation energy. Their deformation experiments at high effective pressures of 300–900 MPa were designed to limit the role of microcracking in the deformation and brittle-plastic interactions in the dislocation creep field and increase the stability of dolomite to higher temperatures. Low strength solid salt assemblies and molten salt cells were employed to obtain higher resolution differential stress measurements than were possible with earlier solid-medium piston-cylinder methods. The flow law parameters reported for dislocation creep are $Q = 145 \pm 20$ kJ/mol and $n = 3.0 \pm 0.1$ (Holyoke et al., 2013). Surprisingly, their activation energy for dislocation creep is lower than $Q = 280 \pm 45$ and 368 $\pm$ 25 kJ/mol determined for diffusion creep (Davis et al., 2008; Delle Piane et al., 2008). The inversion of activation energy between dislocation and diffusion creep for dolomite aggregates is quite unusual, as it is generally expected that rate-limiting mechanisms of intracrystalline deformation will be controlled by a larger energy landscape (activation barriers) relative to grain boundary processes such as grain boundary sliding and diffusion creep (Poirier, 1985). Numerous experimental studies on deformation have revealed that the activation energy of dislocation creep is higher than that of diffusion creep for most minerals, including common silicates and carbonates such as calcite and magnesite (e.g., Holyoke et al., 2014a; Schmid et al., 1980). Calcite, dolomite and magnesite all crystallize in the same rhombohedral structure with a space group of $R\bar{3}c$ or $R\bar{3}$, implying that their flow stresses are determined mainly by the Ca(Mg)-O bond strength or the magnesium content (e.g., Holyoke et al., 2014a). Deformation experiments indicate that calcite, dolomite and magnesite exhibit a systematic increase in flow stress with respect to the magnesium content in the crystal plasticity, dislocation creep and diffusion creep regimes (Holyoke et al., 2014a; Xu et al., 2009); activation energy values of calcite and magnesite are comparable for both dislocation and diffusion creep, and their activation energy values of dislocation creep are higher than those of diffusion creep (Holyoke et al., 2014a; Schmid et al., 1980).

One major cause for the low activation energy value of dislocation creep for Madoc dolomite may be its small field of dislocation creep (Davis et al., 2008; Holyoke et al., 2013). The onset of dislocation creep of Fangshan dolomite starts at lower temperatures than those reported for Madoc dolomite, possibly because the LTP strengths of medium-grained Fangshan dolomite are higher than the LTP strengths of coarser-grained Madoc dolomite. With a stress exponent of $n = 26 \pm 6$, the deformation of Madoc dolomite at 800°C appears to be transitional between LTP and dislocation creep. Holyoke et al. (2013) derived a low value of activation energy $Q = 145$ kJ/mol for dislocation creep of Madoc dolomite from determinations of Q/n (48.3 kJ/mol) using data over 800–1,000°C and stress exponent n (3.0) using data at $T = 900$°C. If, on the one hand, their data at 900 and 1,000°C are used to determine Q/n, removing transitional mechanical behavior at $T = 800$°C, the temperature dependence of stress gives a larger Q/n value of 79.6 kJ/mol, much closer to our Q/n determination of 92 kJ/mol. We also note that Holyoke et al. (2013) determined the stress exponent n, by a slope determination at $T = 900$°C, excluding two experiments at the highest stresses and strain rates that they judged to be transitional between LTP and dislocation creep. If, on the other hand, we include all of their data, a value of n of 3.7 $\pm$ 0.1 is determined, approaching our experimental determination of n. If we use these values from the Holyoke et al. (2013) study, we obtain an activation energy Q for

dislocation creep of 295 kJ/mol, not in coincidence with our Q determination for Fangshan dolomite, but closer in magnitude. Further, this value for dislocation creep does not obviously exceed the activation energy ($Q = 280 \pm 45$ kJ/mol) for diffusion creep of dolomite reported by Davis et al. (2008).

Potential secondary deformation mechanisms or differing combinations of deformation mechanisms that operated in the dislocation regime are also likely to cause differences in flow parameters for dislocation creep of dolomite. Both present deformation experiments and those by Davis et al. (2008) were conducted with high-resolution gas-medium apparatuses under limited confining pressures of 300 or 400 MPa. The differential stresses of the Madoc and Fangshan dolomites were generally larger than the effective pressures, which were only 300 MPa or less than 300 MPa (see Tables 2 and 3). Thus, some microcracking can be anticipated, accompanying dislocation processes. In addition, at temperatures above 800°C, dolomite samples dissociated to generate fine-grained calcite and periclase, and dynamic recrystallization occurred. While the amount of dolomite dissociation to fine-grained products is small at T = 800°C–850°C (this study and Davis et al., 2008) and restricted to original grain boundary regions, the amount of fine-grained products must be larger at T = 900°C, and larger CO_2 pore pressures further reduce the effective pressure of the experiment. Microcracking could contribute to decreasing bulk determinations of Q/n and increasing bulk determinations of stress exponent n because frictional sliding of microcracks is much less sensitive to temperature and rate of deformation than dislocation creep processes, whereas diffusion creep and grain boundary sliding in pockets of fine-grained recrystallized dolomite or reactant products calcite and periclase, which operate concurrently with dislocation creep, could lead to a modified larger bulk temperature dependence of creep (Q/n slope) and lower apparent value of stress exponent n. The stress exponent values of $n = 5.4$ at T = 800°C and $n = 3.8$ at T = 850°C–900°C show a trend that suggests that dolomite dissociation and dynamic recrystallization affect the mechanical results. Griggs apparatus has the advantage of achieving a higher confining pressure than gas-medium apparatus. Deformation experiments by Holyoke et al. (2013) were conducted with the Griggs apparatus at effective pressures of 300–900 MPa, which are higher than the differential stresses of Madoc dolomite, thereby minimizing the potential contributions of microcracking and significantly reducing the generation of fine-grained calcite and periclase reaction products. However, the effect of diffusion creep due to dolomite dissociation and dynamic recrystallization could not be excluded completely in the dislocation creep regime, as indicated by the strain weakening observed in the stress-strain curves for experiments at temperatures of 900°C–1,000°C. In addition, the stress resolution of the Griggs apparatus (±30 MPa for the solid salt assembly, Holyoke et al., 2013) is a matter of concern, which might introduce some uncertainty in the determinations of flow parameters for dislocation creep.

In general, differences in flow parameters for dislocation creep of dolomite determined in this study and previous studies by Davis et al. (2008) and Holyoke et al. (2013) can be largely explained by the small field of dislocation creep for Madoc dolomite, which was not well characterized previously, and potential secondary deformation mechanisms (microcracking, dolomite dissociation, and dynamic recrystallization) that operated with dislocation creep. Other causes might include confining pressure (activation volume), microstructure, and stress resolution, but their effects are speculated to be less significant. In the present study, the deformation experiments were performed by a gas-medium Paterson apparatus with high stress resolution, and the rheological parameters of dislocation creep for Fangshan dolomite were derived by mechanical data in the dislocation creep regime in which dislocation creep is predominant; hence, the rheological results of dolomite aggregates should be reliable. The activation energy of dislocation creep determined in this study agrees well with that from Davis et al. (2008) and is comparable to the activation energy values of dislocation creep for Carrara marble ($Q = 428$ kJ/mol) (Schmid et al., 1980) and magnesite ($Q = 410$ kJ/mol) (Holyoke et al., 2014a). Our results indicate that the activation energy value of dislocation creep for dolomite aggregates is much higher than that of diffusion creep ($Q = 280$ kJ/mol, Davis et al., 2008; $Q = 368$ kJ/mol, Delle Piane et al., 2008) and hence does not support the inversion of activation energy between dislocation and diffusion creep.

4.5. Geological Implications

Our experimental results for Fangshan dolomite can be applied to natural deformation in the crust, using flow laws for crystal-plastic deformation at low temperature with an exponential relationship and

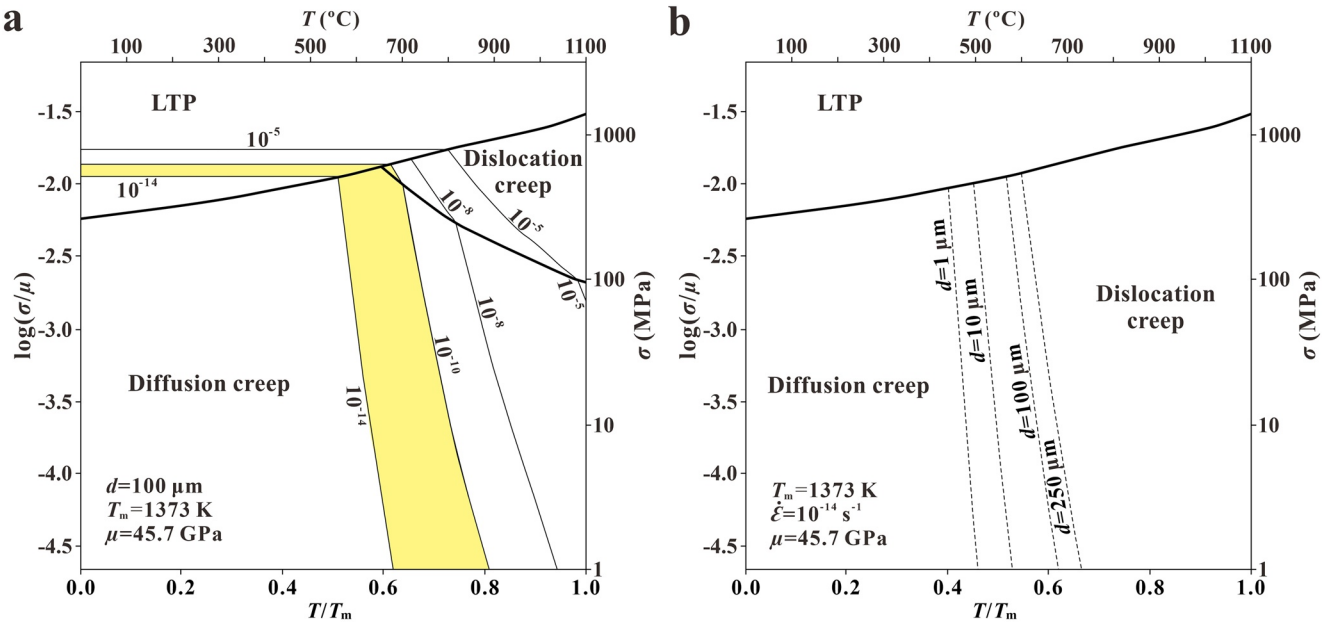

Figure 14. (a) Deformation mechanism map for dolomite with a grain size d = 100 μm, constructed using the flow laws of LTP and dislocation creep determined in this study and the flow law of diffusion creep reported by Davis et al. (2008), which suggests that over most geological strain rates (10^{-10} to 10^{-14} s^{-1}), LTP dominates at temperatures <650°C and high differential stress and that diffusion creep is the dominant deformation mechanism at temperatures >560°C and low differential stress. (b) Decreasing the grain size of dolomite shifts the boundary between dislocation and diffusion creep to lower temperatures and shifts the onset of dislocation creep from LTP to lower temperatures. The temperature is normalized by a melting temperature of T_m = 1373 K (metastable extension from high-pressure measurements, Wyllie & Huang, 1976), and the flow stress is normalized by a shear modulus of μ = 45.7 GPa (Bass, 1995). LTP, low-temperature plasticity.

dislocation creep at high temperature with a power relationship. Our predictions of dolomite strength differ from those of Davis et al. (2008) and Holyoke et al. (2013) according to differing values of n and Q. To predict the deformation mechanisms dominating the rheology of medium-grained dolomite aggregates within the Earth, the low-temperature exponential law and high-temperature dislocation flow law determined in this study and that reported for diffusion creep of fine-grained synthetic dolomite aggregates (Davis et al., 2008) are combined to define a deformation mechanism map for dolomite aggregates with a grain size of 100 μm in logarithmic stress versus T/T_m space (Figure 14a), where T_m is the melting point of dolomite (Wyllie & Huang, 1976). Our deformation mechanism map is similar to that from Davis et al. (2008) but has a slightly steeper dislocation creep-diffusion creep boundary due to the relatively greater temperature dependence of flow stress for Fangshan dolomite than Madoc dolomite. As shown in Figure 14a, three fields are defined in the deformation mechanism map for dolomite with LTP at high stresses, dislocation creep at high temperature and relatively high stresses, and diffusion creep at low stresses and elevated temperature. Crystal plasticity and twinning dominate the deformation of dolomite at very high stresses, nearly independent of the strain rate. From laboratory to nature, for instance, a several orders-of-magnitude difference in strain rate does not result in a large difference in flow stress in the LTP regime. The flow stress increases slightly with increasing temperature in this regime, corresponding to the thermal increase in the CRSS of c-slip (Figure 12; Barber et al., 1981). This is unusual relative to the generally accepted temperature dependence of flow stress for common rock-forming minerals (such as quartz and olivine), although such thermal hardening was previously reported by Davis et al. (2008) for Madoc dolomite deformed at $T \leq 700$°C, by Higgs and Handin (1959) and Barber et al. (1981) for oriented single crystals of dolomite, and by earlier works (e.g., Ardley, 1955; Davis & Stoloff, 1965; Lawley et al., 1961; Stoloff & Davies, 1964) for alloys with order-disorder or lattice anisotropy. One possible interpretation by Barber et al. (1981) is that thermal hardening is limited to basal (c) slip, and during dislocation movement, the increase in friction of CO_3^{2-} groups increases with thermal vibration, expansion and rotation of CO_3^{2-} groups. However, there is no similar thermal hardening found in calcite (e.g., Barber et al., 2007, 1981; de Bresser & Spiers, 1997) with a crystal structure similar to dolomite. Therefore, further research is needed to explore the reasons behind this behavior.

Extrapolated to natural conditions, for dolomite aggregates with a grain size of 100 μm deformed over most geological strain rates (10^{-10} to 10^{-14} s^{-1}), LTP dominates at temperatures ≤~560°C. At temperatures between 560 and 650°C, the deformation of dolomites is dominated by LTP at relatively high differential stresses and by diffusion creep at low stresses (Figure 14a). When $T > 650$°C, however, diffusion creep is the dominant deformation mechanism, likely accompanied by a small amount of LTP and dislocation creep deformation. Given a specific strain rate (10^{-14} s^{-1}) for the deformation of dolomite in nature, a change in grain size shifts the diffusion creep-dislocation creep boundary to higher temperatures for coarse grain sizes developed during grain growth or to lower temperatures when grain size is refined by recrystallization (Figure 14b). Depending on grain size, the extent of the dislocation creep field is limited to high temperatures and relatively high stresses ($T >$ ~460°C for $d = 1$ μm, $T >$ ~500°C for $d = 10$ μm, $T >$ ~560°C for $d = 100$ μm, and $T >$ ~600°C for $d = 250$ μm). This means that dislocation creep is expected to occur under a relatively narrow set of geological conditions of high stress and high temperature; instead, diffusion creep is expected to dominate the deformation of dolomite over most geological strain rates and low tectonic stress environments. On the basis of a comparison of grain sizes and CPOs of dolomite and calcite at 390–700°C, Berger et al. (2016) recently concluded that dolomite deformation is dominated by dislocation creep at $T >$ ~500°C when the grain size is greater than ~100 μm. This is consistent with the prediction from our deformation mechanism map, where dislocation creep is the dominant deformation mechanism when $T >$ ~560°C for a 100 μm grain size (Figure 14b).

5. Conclusions

Triaxial compression experiments were performed on medium-grained Fangshan dolomite at effective pressures of ~50–300 MPa, temperatures of 27°C–900°C, and strain rates from 10^{-6} s^{-1} to 2×10^{-4} s^{-1}. Analysis of the mechanical data and deformation microstructures reveals three different deformation regimes: LTP at temperatures of $T \leq 500$°C (Regime 1), dislocation creep at $T \geq 800$°C (Regime 2), and a transitional field between LTP and dislocation creep at 500°C $< T \leq$ 800°C (Regime 3). The LTP regime is characterized by microstructures of predominant abrupt undulatory extinctions and f-twins and weak dependencies of the flow stress on the strain rate (high stress exponent $n =$ ~70–78) and temperature. The flow behavior of Fangshan dolomite in the LTP regime can be expressed by an exponential constitutive equation $\dot{\varepsilon} = \dot{\varepsilon}_0 \times \exp(\alpha \times \sigma)$, and the rheological parameters are determined as $\alpha = 0.0806 \pm 0.0078$ and $\ln \dot{\varepsilon}_0 = -76.66 \pm 6.24$. The dislocation creep regime shows characteristic microstructures of smooth undulating extinction and new recrystallized grains and features significant dependencies of the flow stress on the strain rate (low stress exponent $n =$ ~3.8–5.4) and temperature, which can be described by a power law relationship $\dot{\varepsilon} = A\sigma^n \exp\left(\frac{-Q}{RT}\right)$. Fitting the mechanical data of Fangshan dolomite deformed in the dislocation creep regime yields the rheological parameters of the stress exponent $n = 4.75 \pm 0.58$, activation energy $Q = 436 \pm 54$ kJ/mol and preexponential factor $\log A = 3.48 \pm 1.41$.

Medium-grained Fangshan dolomite exhibits rheological behavior quite similar to that of coarse-grained Madoc dolomite. However, the onset temperature of the dislocation creep regime for the Fangshan dolomite is approximately 50–100°C lower than that for the Madoc dolomite, which allows us to determine the rheological parameters of the dolomite dislocation creep over a wider range of conditions. The activation energy of dislocation creep determined in this study is much higher than that of diffusion creep for dolomite aggregates reported previously and hence does not support an inversion of activation energy between dislocation and diffusion creep. Our flow laws of LTP and dislocation creep regimes for medium-grained Fangshan dolomite are combined with the flow law of diffusion creep for fine-grained synthetic dolomite reported in a previous study to construct a deformation mechanism map for dolomite. Under natural conditions (strain rates), the LTP regime is inferred to occur at high stress and low temperature, dislocation creep occurs at high temperature and relatively high stress, and diffusion creep occurs at moderate-high temperature and low stress. The dislocation creep-diffusion creep boundary shifts to higher temperatures when coarsening (i.e., increasing grain size). It is expected that dislocation creep is limited to a relatively narrow set of conditions, or high temperature and high stress, whereas diffusion creep dominates the deformation of dolomite in tectonic settings characterized by common geological strain rates and low stress.

Data Availability Statement

Original data for supporting the analysis and conclusions are accessible through the Mendeley repository (http://dx.doi.org/10.17632/hmmt2797yk.1).

Acknowledgments
We sincerely appreciate the critical and constructive comments from Matteo Demurtas and Andreas Kronenberg and the Editor Douglas Schmitt, who helped us improve the manuscript. Guinan Zhang is thanked for helping during some deformation experiments. Professor Yongsheng Zhou is gratefully acknowledged for critical comments on an early version of this manuscript. This work was supported by the Strategic Priority Research Program (B) of the Chinese Academy of Sciences (Grant No. XDB18000000), the National Natural Science Foundation of China (Grant Nos. 41572198, 41702224, 41874107, and 41574079), the Pearl River Talent Plan of Guangdong Province, and the research grant of the State Key Laboratory of Earthquake Dynamics (Grant No. LED2017B06). This is a contribution to No. IS-3009 from the GIGCAS.

References

Ardley, G. W. (1955). On the effect of ordering upon the strength of Cu3Au. *Acta Metallurgica*, *3*, 525–532. https://doi.org/10.1016/0001-6160(55)90110-3

Austin, N., & Evans, B. (2009). The kinetics of microstructural evolution during deformation of calcite. *Journal of Geophysical Research*, *114*, B09402. https://doi.org/10.1029/2008JB006138

Austin, N. J., & Kennedy, L. A. (2005). Textural controls on the brittle deformation of dolomite: variations in peak strength. In D. Gapais, J. P. Brun, & P. R. Cobbold (Eds.), *Deformation mechanisms, rheology and tectonics: From minerals to the lithosphere* (Vol. 243, pp. 37–49). London: Geological Society, London, Special Publications. https://doi.org/10.1144/gsl.sp.2005.243.01.05

Austin, N. J., Kennedy, L. A., Logan, J. M., & Rodway, R. (2005). Textural controls on the brittle deformation of dolomite: the transition from brittle faulting to cataclastic flow. In D. Gapais, J. P. Brun, & P. R. Cobbold (Eds.), *Deformation mechanisms, rheology and tectonics: From minerals to the lithosphere* (Vol. 243, pp. 51–66). London: Geological Society, London, Special Publications. https://doi.org/10.1144/gsl.sp.2005.243.01.06

Barber, D. J., Freeman, L. A., & Smith, D. J. (1983). Analysis of high-voltage, high-resolution images of lattice defects in experimentally-deformed dolomite. *Physics and Chemistry of Minerals*, *9*, 102–108. https://doi.org/10.1007/BF00308365

Barber, D. J., Heard, H. C., & Wenk, H. R. (1981). Deformation of dolomite single crystals from 20–800°C. *Physics and Chemistry of Minerals*, *7*, 271–286. https://doi.org/10.1007/BF00311980

Barber, D. J., & Wenk, H.-R. (1979). Deformation twinning in calcite, dolomite, and other rhombohedral carbonates. *Physics and Chemistry of Minerals*, *5*, 141–165. https://doi.org/10.1007/BF00307550

Barber, D. J., & Wenk, H.-R. (2001). Slip and dislocation behavior in dolomite. *European Journal of Mineralogy*, *13*, 221–243. https://doi.org/10.1127/0935-1221/01/0013-0221

Barber, D. J., Wenk, H.-R., Gomez-Barreiro, J., Rybacki, E., & Dresen, G. (2007). Basal slip and texture development in calcite: New results from torsion experiments. *Physics and Chemistry of Minerals*, *34*, 73–84. https://doi.org/10.1007/s00269-006-0129-3

Barber, D. J., Wenk, H.-R., & Heard, H. C. (1994). The plastic deformation of polycrystalline dolomite: Comparison of experimental results with theoretical predictions. *Materials Science and Engineering: A*, *175*, 83–104. https://doi.org/10.1016/0921-5093(94)91048-0

Bass, J. D. (1995). Elasticity of minerals, glasses and melts. In T. J. Ahrens (Ed.), *Mineral physics and crystallography. A handbook of physical constants* (pp. 45–63). Washington, DC: AGU.

Berger, A., Ebert, A., Ramseyer, K., Gnos, E., & Decrouez, D. (2016). Dolomite microstructures between 390° and 700°C: Indications for deformation mechanisms and grain size evolution. *Journal of Structural Geology*, *89*, 144–152. https://doi.org/10.1016/j.jsg.2016.06.001

Berg, G. W. (1986). Evidence for carbonate in the mantle. *Nature*, *324*, 50–51. https://doi.org/10.1038/324050a0

Bestmann, M., Kunze, K., & Matthews, A. (2000). Evolution of a calcite marble shear zone complex on Thassos Island, Greece: Microstructural and textural fabrics and their kinematic significance. *Journal of Structural Geology*, *22*, 1789–1807. https://doi.org/10.1016/s0191-8141(00)00112-7

Brenker, F. E., Vollmer, C., Vincze, L., Vekemans, B., Szymanski, A., Janssens, K., et al. (2007). Carbonates from the lower part of transition zone or even the lower mantle. *Earth and Planetary Science Letters*, *260*(1–2), 1–9. https://doi.org/10.1016/j.epsl.2007.02.038

Buob, A., Luth, R. W., Schmidt, M. W., & Ulmer, P. (2006). Experiments on $CaCO_3$-$MgCO_3$ solid solutions at high pressure and temperature. *American Mineralogist*, *91*(2–3), 435–440. https://doi.org/10.2138/am.2006.1910

Davis, N. E., Kronenberg, A. K., & Newman, J. (2008). Plasticity and diffusion creep of dolomite. *Tectonophysics*, *456*, 127–146. https://doi.org/10.1016/j.tecto.2008.02.002

Davis, R. G., & Stoloff, N. S. (1965). On the yield stress of aged Ni-Al alloys. *Transactions of the Metallurgical Society of AIME*, *233*, 714–719.

de Bresser, J. H. P. (2002). On the mechanism of dislocation creep of calcite at high temperature: Inferences from experimentally measured pressure sensitivity and strain rate sensitivity of flow stress. *Journal of Geophysical Research*, *107*(B12), 2337. https://doi.org/10.1029/2002JB001812

de Bresser, J. H. P., & Spiers, C. J. (1997). Strength characteristics of the r, f, and c slip systems in calcite. *Tectonophysics*, *272*, 1–23. https://doi.org/10.1016/s0040-1951(96)00273-9

de Bresser, J. H. P., Urai, J. L., & Olgaard, D. L. (2005). Effect of water on the strength and microstructure of Carrara marble axially compressed at high temperature. *Journal of Structural Geology*, *27*(2), 265–281. https://doi.org/10.1016/j.jsg.2004.10.002

Delle Piane, C., Burlini, L., Kunze, K., Brack, P., & Burg, J. P. (2008). Rheology of dolomite: Large strain torsion experiments and natural examples. *Journal of Structural Geology*, *30*, 767–776. https://doi.org/10.1016/j.jsg.2008.02.018

Eggler, D. H., Kushiro, I., & Holloway, J. R. (1976). Stability of carbonate minerals in a hydrous mantle. Carnegie Institution of Washington, Year Book.

Freund, D., Wang, Z. C., Rybacki, E., & Georg, D. (2004). High-temperature creep of synthetic calcite aggregates: Influence of Mn-content. *Earth and Planetary Science Letters*, *226*(3–4), 433–448. https://doi.org/10.1016/j.epsl.2004.06.020

Goldsmith, J. R. (1959). Some aspects of the geochemistry of carbonates. In P. H. Abelson (Ed.), *Researches in geochemistry* (Vol. 1, pp. 336–358). New York, NY: John Wiley & Sons.

Goto, A., Kunugiza, K., & Omori, S. (2007). Evolving fluid composition during prograde metamorphism in subduction zones: A new approach using carbonate-bearing assemblages in the pelitic system. *Gondwana Research*, *11*(1–2), 166–179. https://doi.org/10.1016/j.gr.2006.07.006

Gratier, J.-P., Richard, J., Renard, F., Mittempergher, S., Doan, M.-L., Di Toro, G., et al. (2011). Aseismic sliding of active faults by pressure solution creep: Evidence from the San Andreas Fault Observatory at Depth. *Geology*, *39*(12), 1131–1134. https://doi.org/10.1130/g32073.1

Griggs, D., & Miller, W. B. (1951). Deformation of Yule Marble. Part I: Compression and extension experiments on dry yule marble at 10,000 atmospheres confining pressure, room temperature. *Geological Society of America Bulletin*, *62*, 853–862. https://doi.org/10.1130/0016-7606(1951)62[853:DOYMPI]2.0.CO;2

Griggs, D., Turner, F. J., Borg, I., & Sosoka, J. (1953). Deformation of Yule Marble. Part V: Effects at 300°C. *Geological Society of America Bulletin*, *64*, 1327–1342. https://doi.org/10.1130/0016-7606(1953)64[1327:DOYMPV]2.0.CO;2

Handin, J., & Fairbairn, H. W. (1955). Experimental deformation of Hasmark dolomite. *Geological Society of America Bulletin*, *66*, 1257–1274. https://doi.org/10.1130/0016-7606(1955)66[1257:EDOHD]2.0.CO;2

Handin, J. W., & Griggs, D. (1951). Deformation of Yule Marble. Part Ii: Predicted fabric changes. *Geological Society of America Bulletin*, *62*, 863–886. https://doi.org/10.1130/0016-7606(1951)62[863:DOYMPI]2.0.CO;2

Heard, H. C. (1976). Comparison of the flow properties of rocks at crustal conditions. *Philosophical Transactions of the Royal Society of London*, *283*, 173–186.

Heard, H. C., & Raleigh, C. B. (1972). Steady-state flow in Marble at 500° to 800°C. *Geological Society of America Bulletin*, *83*, 935–956. https://doi.org/10.1130/0016-7606(1972)83[935:SFIMAT]2.0.CO;2

Herwegh, M., de Bresser, J. H. P., & ter Heege, J. H. (2005). Combining natural microstructures with composite flow laws: An improved approach for the extrapolation of lab data to nature. *Journal of Structural Geology*, *27*, 503–521. https://doi.org/10.1016/j.jsg.2004.10.010

Herwegh, M., Xiao, X., & Evans, B. (2003). The effect of dissolved magnesium on diffusion creep in calcite. *Earth and Planetary Science Letters*, *212*(3), 457–470. https://doi.org/10.1016/s0012-821x(03)00284-x

Higgs, D. V., & Handin, J. (1959). Experimental deformation of dolomite single crystals. *Geological Society of America Bulletin*, *70*, 245–278. https://doi.org/10.1130/0016-7606(1959)70[245:EDODSC]2.0.CO;2

Holyoke, C. W., Kronenberg, A. K., & Newman, J. (2013). Dislocation creep of polycrystalline dolomite. *Tectonophysics*, *590*, 72–82. https://doi.org/10.1016/j.tecto.2013.01.011

Holyoke, C. W., Kronenberg, A. K., & Newman, J. (2014). Microstructural evolution during strain localization in dolomite aggregates. *Journal of Structural Geology*, *69*, 449–464. https://doi.org/10.1016/j.jsg.2014.04.008

Holyoke, C. W., Kronenberg, A. K., Newman, J., & Ulrich, C. (2014). Rheology of magnesite. *Journal of Geophysical Research: Solid Earth*, *119*, 6534–6557. https://doi.org/10.1002/2013JB010541

Isshiki, M., Irifune, T., Hirose, K., Ono, S., Ohishi, Y., Watanuki, T., et al. (2004). Stability of magnesite and its high-pressure form in the lowermost mantle. *Nature*, *427*, 60–63. https://doi.org/10.1038/nature02181

Lawley, A., Vidoz, E. A., & Cahn, R. W. (1961). The dependence of the flow stress of Fe3Al on crystallographic order. *Acta Metallurgica*, *9*, 287–296. https://doi.org/10.1016/0001-6160(61)90221-8

Li, J. F., Song, M. S., Shao, T. B., Xia, Y., Wang, Q., & Zhou, W. (2013). Correction for the axial deformation data recorded by Paterson-type gas medium high-pressure high temperature machine(in Chinese with English abstract). *Geotectonica et Metallogenia*, *37*(1), 127–137.

Luth, R. W. (2001). Experimental determination of the reaction aragonite + magnesite = dolomite at 5 to 9 GPa. *Contributions to Mineralogy and Petrology*, *141*(2), 222–232. https://doi.org/10.1007/s004100100238

Merlini, M., Crichton, W. A., Hanfland, M., Gemmi, M., Müller, H., Kupenko, I., & Dubrovinsky, L. (2012). Structures of dolomite at ultrahigh pressure and their influence on the deep carbon cycle. *Proceedings of the National Academy of Sciences of the United States of America*, *109*, 13509–13514. https://doi.org/10.1073/pnas.1201336109

Neumann, E.-R. (1969). Experimental recrystallization of dolomite and comparison of preferred orientations of calcite and dolomite in deformed rocks. *The Journal of Geology*, *77*, 426–438. https://doi.org/10.1086/628368

Paterson, M. S. (1970). A high-pressure, high-temperature apparatus for rock deformation. *International Journal of Rock Mechanics and Mining Sciences & Geomechanics Abstracts*, *7*(5), 517–526. https://doi.org/10.1016/0148-9062(70)90004-5

Poirier, J. P. (1985). *Creep of crystals: High-temperature deformation processes in Metals, ceramics, and minerals*. Cambridge, UK:Cambridge University Press.

Renner, J., Evans, B., & Siddiqi, G. (2002). Dislocation creep of calcite. *Journal of Geophysical Research*, *107*(B12), 2364. https://doi.org/10.1029/2001JB001680

Rutter, E. H. (1972). The influence of interstitial water on the rheological behavior of calcite rocks. *Tectonophysics*, *14*, 13–33. https://doi.org/10.1016/0040-1951(72)90003-0

Rutter, E. H. (1974). The influence of temperature, strain rate and interstitial water in the experimental deformation of calcite rocks. *Tectonophysics*, *22*, 311–334. https://doi.org/10.1016/0040-1951(74)90089-4

Rybacki, E., Evans, B., Janssen, C., Wirth, R., & Dresen, G. (2013). Influence of stress, temperature, and strain on calcite twins constrained by deformation experiments. *Tectonophysics*, *601*, 20–36. https://doi.org/10.1016/j.tecto.2013.04.021

Rybacki, E., Janssen, C., Wirth, R., Chen, K., Wenk, H.-R., Stromeyer, D., & Dresen, G. (2011). Low-temperature deformation in calcite veins of SAFOD core samples (San Andreas Fault)—Microstructural analysis and implications for fault rheology. *Tectonophysics*, *509*(1–2), 107–119. https://doi.org/10.1016/j.tecto.2011.05.014

Sato, K., & Katsura, T. (2001). Experimental investigation on dolomite dissociation into aragonite+magnesite up to 8.5 GPa. *Earth and Planetary Science Letters*, *184*, 529–534. https://doi.org/10.1016/s0012-821x(00)00346-0

Schmid, S. M., Boland, J. N., & Paterson, M. S. (1977). Superplastic flow in finegrained limestone. *Tectonophysics*, *43*, 257–291. https://doi.org/10.1016/0040-1951(77)90120-2

Schmid, S. M., Paterson, M. S., & Boland, J. N. (1980). High temperature flow and dynamic recrystallization in Carrara marble. *Tectonophysics*, *65*, 245–280. https://doi.org/10.1016/0040-1951(80)90077-3

Shao, T. B., Ji, S. C., Li, J. F., Wang, Q., & Song, M. S. (2011). Paterson gas-medium high-pressure high-temperature testing system and its applications in rheology of rocks. *Geotectonica et Metallogenia*, *35*(3), 457–476.

Shirasaka, M., Takahashi, E., Nishihara, Y., Matsukage, K., & Kikegawa, T. (2002). In situ X-ray observation of the reaction dolomite = aragonite + magnesite at 900–1300 K. *American Mineralogist*, *87*, 922–930. https://doi.org/10.2138/am-2002-0715

Song, M. S., Shao, T. B., Li, J. F., Ji, S. C., & Wang, Q. (2014). Experimental study of deformation of Carrara marble at high pressure and high temperature. *Acta Petrologica Sinica*, *30*(2), 589–596.

Stoloff, N. S., & Davies, R. G. (1964). The effect of ordering on the plastic deformation of Mg_3Cd. *Transactions of American Society of Metals*, *57*, 247–260.

Thomson, A. R., Walter, M. J., Kohn, S. C., & Brooker, R. A. (2016). Slab melting as a barrier to deep carbon subduction. *Nature*, *529*, 76–79. https://doi.org/10.1038/nature16174

Turner, F. J., Griggs, D. T., Clark, R. H., & Dixon, R. H. (1956). Deformation of Yule Marble. Part Vii: Development of oriented fabrics at 300°C–500°C. *Geological Society of America Bulletin*, *67*, 1259–1294. https://doi.org/10.1130/0016-7606(1956)67[1259:DOYMPV]2.0.CO;2

Turner, F. J., Griggs, D. T., Heard, H. C., & Weiss, L. W. (1954). Plastic deformation of dolomite rock at 380 degrees C. *American Journal of Science*, *252*, 477–488. https://doi.org/10.2475/ajs.252.8.477

Ulrich, S., Schulmann, K., & Casey, M. (2002). Microstructural evolution and rheological behavior of marbles deformed at different crustal levels. *Journal of Structural Geology*, *24*, 979–995. https://doi.org/10.1016/s0191-8141(01)00132-8

Walker, A. N., Rutter, E. H., & Brodie, K. H. (1990). Experimental study of grain-size sensitive flow of synthetic, hot-pressed calcite rocks. In R. J. Knipe, & E. H. Rutter (Eds.), *Deformation mechanisms, rheology and tectonics* (Vol. 54, pp. 259–284).London: Geological Society, London, Special Publications. https://doi.org/10.1144/gsl.sp.1990.054.01.24

Wyllie, P. J., & Huang, W.-L. (1976). Carbonation and melting reactions in the system CaO–MgO–SiO_2–CO_2 at mantle pressures with geophysical and petrological applications. *Contributions to Mineralogy and Petrology*, *54*, 79–107. https://doi.org/10.1007/BF00372117

Xu, L., & Evans, B. (2010). Strain heterogeneity in deformed Carrara marble using a microscale strain mapping technique. *Journal of Geophysical Research*, *115*, B04202. https://doi.org/10.1029/2009JB006458

Xu, L., Renner, J., Herwegh, M., & Evans, B. (2009). The effect of dissolved magnesium on creep of calcite II: Transition from diffusion creep to dislocation creep. *Contributions to Mineralogy and Petrology*, *157*(3), 339–358. https://doi.org/10.1007/s00410-008-0338-5

Zhang, L., Ellis, D. J., Arculus, R. J., Jiang, W., & Wei, C. (2003). 'Forbidden zone' subduction of sediments to 150 km depth- the reaction of dolomite to magnesite + aragonite in the UHPM metapelites from western Tianshan, China. *Journal of Metamorphic Geology*, *21*, 523–529. https://doi.org/10.1046/j.1525-1314.2003.00460.x

Zhang, Y. H., Zhou, Y. S., Yao, W. M., He, C. R., & Dang, J. X. (2017). Experimental study on the effect of water on the strength and deformation mechanism of Carrara marble at high temperature. *Seismology and Geology*, *39*(1), 753. https://doi.org/10.3969/j.issn.0253-4967.2017.01

Zhang, Y. Y., & Zhou, Y. S. (2012). The strength and deformation mechanisms of brittle-plastic transition zone, and the effects of strain rate and fluids. *Seismology and Geology*, *34*(1), 172–194.

Zhu, Y., & Ogasawara, Y. (2002). Carbon recycled into deep Earth: Evidence from dolomite dissociation in subduction-zone rocks. *Geology*, *30*(10), 947–950. https://doi.org/10.1130/0091-7613(2002)030<0947:CRIDEE>2.0.CO;2